Kinetics of H_2-O_2-H_2O redox equilibria and formation of metastable H_2O_2 under low temperature hydrothermal conditions

Dionysis I. Foustoukos[1*], Jennifer L. Houghton[2] , William E. Jr. Seyfried[3], Stefan M. Sievert[4] and George D. Cody[1]

[1]*Geophysical Laboratory, Carnegie Institution of Washington, 5251 Broad Branch Rd. NW, Washington DC 20015*

[2]*Environmental Science Program, Rhodes College, Memphis,TN 38112*

[3]*Department of Geology, University of Minnesota, 310 Pillsbury Drive SE, Minneapolis, MN 55455*

[4] *Department of Biology, Woods Hole Oceanographic Institution, Woods Hole, MA 02543*

**Correspondence author: dfoustoukos@ciw.edu*

Keywords: Knallgas reaction, H_2 oxidation, metastable hydrogen peroxide, anaerobic chemolithoautotrophic metabolism, Fenton reaction, hydrothermal systems

Running Title: Kinetics of H_2-O_2-H_2O equilibria and formation of metastable H_2O_2

ABSTRACT

Hydrothermal experiments were conducted to evaluate the kinetics of $H_{2(aq)}$ oxidation in the homogeneous H_2-O_2-H_2O system at conditions reflecting subsurface/near-seafloor hydrothermal environments (55-250 ^{o}C and 242-497 bar). The kinetics of the water-forming reaction that controls the fundamental equilibrium between dissolved $H_{2(aq)}$ and $O_{2(aq)}$, are expected to impose significant constraints on the redox gradients that develop when mixing occurs between oxygenated seawater and high-temperature anoxic vent fluid at near-seafloor conditions. Experimental data indicate that, indeed, the kinetics of $H_{2(aq)}$-$O_{2(aq)}$ equilibrium become slower with decreasing temperature, allowing excess $H_{2(aq)}$ to remain in solution. Sluggish reaction rates of $H_{2(aq)}$ oxidation suggest that active microbial populations in near-seafloor and subsurface environments could potentially utilize both $H_{2(aq)}$ and $O_{2(aq)}$, even at temperatures lower than 40 ^{o}C due to $H_{2(aq)}$ persistence in the seawater/vent fluid mixtures. For these H_2-O_2 disequilibrium conditions, redox gradients along the seawater/hydrothermal fluid mixing interface are not sharp and microbially-mediated $H_{2(aq)}$ oxidation coupled with a lack of other electron acceptors (e.g. nitrate) could provide an important energy source available at low-temperature diffuse flow vent sites.

More importantly, when $H_{2(aq)}$-$O_{2(aq)}$ disequilibrium conditions apply, formation of metastable hydrogen peroxide is observed. The yield of $H_2O_{2(aq)}$ synthesis appears to be enhanced under conditions of elevated $H_{2(aq)}/O_{2(aq)}$ molar ratios that correspond to abundant $H_{2(aq)}$ concentrations. Formation of metastable H_2O_2 is expected to affect the distribution of dissolved organic carbon (DOC) owing to the existence of an additional strong oxidizing agent. Oxidation of magnetite and/or Fe^{++} by hydrogen peroxide could also induce formation of metastable hydroxyl radicals (•OH) through Fenton-type

reactions, further broadening the implications of hydrogen peroxide in hydrothermal environments.

1. Introduction

Low-temperature diffuse fluid flow in submarine hydrothermal systems represents an important mechanism of heat and mass transfer in mid-ocean ridges, playing a key role in the re-distribution of volatiles and metals. In general, diffuse flow systems involve subseafloor mixing between oxygenated cold seawater and high-temperature anoxic hydrothermal fluid (CORLISS et al., 1979; EDMOND et al., 1979). The contrasting chemical and physical conditions of these two fluid sources induce sharp gradients, with important implications for the distribution of redox- and pH-sensitive aqueous species (DING et al., 2001; DING et al., 2005; KELLEY et al., 2002; LUTHER et al., 2001; TIVEY, 1995). Identifying metastable equilibria that likely accompany redox and pH gradients not only helps to elucidate subseafloor hydrothermal alteration processes, but may also contribute important insights into the nature of energy sources fueling a subseafloor biosphere. For example, availability of dissolved oxygen, a major source of metabolic energy for aerobic lithoautotrophs, in the presence of reduced inorganic compounds, influences the distribution of aerobic and anaerobic bacteria in the subsurface (EDWARDS et al., 2005; REYSENBACH and SHOCK, 2002). The existence of hydrogen-utilizing chemolithotrophic bacteria in chimney structures, however, is also consistent with the persistence of $H_{2(aq)}$-enriched fluids at low temperatures ($T < 70\ ^{o}C$) (REYSENBACH et al., 2000).

The distribution of redox couples (e.g. $H_{2(aq)}/O_{2(aq)}$, $H_2S_{(aq)}/SO_4^{--}$) is typically assessed by use of geochemical mixing models constructed assuming complete thermodynamic equilibria or complete disequilibria (MCCOLLOM and SHOCK, 1997; SHOCK and HOLLAND, 2004). A number of experimental and field studies, however, have suggested that these assumptions might be invalid, especially for moderately low

temperatures (< 200 ^{o}C) (DING et al., 2001; FOUSTOUKOS et al., 2009; MCCOLLOM and SEEWALD, 2006). For example, fluid samples collected from diffuse and focused flow vents at the Main Endeavour Field (MEF) along Juan de Fuca Ridge indicate that the types of organic species can be related to the geochemical processes occurring within the seawater-hydrothermal fluid mixing zone (FOUSTOUKOS et al., 2009). In particular, the distribution of dissolved volatiles measured in the high and low-temperature hydrothermal vent fluids at MEF confirms the strong effect of temperature on the kinetics of the CO_2-CO-H_2-H_2O redox equilibria (SEEWALD et al., 2006), where slow CO_2-CO reaction rates are indicated at temperatures less than 50 ^{o}C.

Another important redox couple that can be linked to subsurface mixing processes involves dissolved $H_{2(aq)}$ and $O_{2(aq)}$ species. Theoretical studies have suggested that $H_{2(aq)}$-$O_{2(aq)}$ disequilibrium can provide large energy sources to support microbial metabolism in deep-sea vent environments (MCCOLLOM and SHOCK, 1997; SHOCK and HOLLAND, 2004). At elevated temperature and pressure (350 ^{o}C-350 bar), the water-forming reaction that ultimately constrains this redox couple has been shown to achieve thermodynamic equilibrium rapidly (SEEWALD, 1994). However, at low temperatures only one set of experimental data exists (Table 1) (HOUGHTON, 2003). These data describe $H_{2(aq)}$ oxidation rates at 100 ^{o}C-500 bar in the homogeneous H_2-O_2-H_2O system and support the presence of excess $H_{2(aq)}$ in solution after mixing $H_{2(aq)}$- and $O_{2(aq)}$-enriched aqueous fluids (Table 1). Furthermore, $H_{2(aq)}$-$O_{2(aq)}$ disequilbrium at low temperatures (< 37 ^{o}C) has also been suggested by dissolved oxygen concentrations measured in groundwaters and in experimental studies involving pyrite oxidation (KAMEI and OHMOTO, 2000; LINDBERG and RUNNELLS, 1984), where aqueous solutions maintained elevated $O_{2(aq)}$

concentrations even at highly reducing conditions. Thus, to more closely examine the effect of temperature on $H_{2(aq)}$-$O_{2(aq)}$ equilibrium, a series of hydrothermal experiments were conducted in the homogeneous H_2-O_2-H_2O system, at temperature and pressure conditions reflecting subsurface/near-seafloor hydrothermal environments (55-250 ^{o}C and 242-497 bar). This study also examines the formation of metastable aqueous species. For example, reducing conditions when coupled with disequilibrium between dissolved oxygen and hydrogen, could contribute to the formation of metastable aqueous oxidants (e.g. $H_2O_{2(aq)}$). The formation of such as species could affect redox gradients developed within the seawater-hydrothermal fluid mixing zone with implications not only for the chemical evolution of diffuse flow hydrothermal fluids, but also for the diversity of the near-vent microbial and macrofaunal communities.

2. Methods

2.1 Experimental and Analytical Procedures

To determine $H_{2(aq)}$ oxidation rates at a wide range of temperatures (55-250 ^{o}C), hydrothermal experiments were conducted by using both “open system” flow-through (Geophysical Lab) and “closed system” batch reactors (University of Minnesota) (Table 3, 4). The batch reactor system facilitated determination of equilibrium phase relations, while the flow-though experiments were better suited to assess reaction rates. In effect, a 60 ml flexible Au/Ti cell reaction cell was used to overcome “open system” limitations linked to short reaction times. For example, in the flow-through experimental system, fluid flow rates were adjusted to provide residence times up to 15 minutes. Reaction times up to 1451 minutes were achieved in the flexible Au/Ti cell (Table 3, 4). The latter

experimental design allows time series sampling of internally filtered fluid at experimental conditions (SEYFRIED et al., 1987), while the chemical composition of the reactant fluids can be modified at any time by "in-situ" injection of aqueous solutions directly in the cell through a sampling valve. Thus, the progress of the H_2-O_2 redox equilibrium can be monitored and controlled. However, to evaluate reaction kinetics that exhibit short half-life (e.g. few minutes) use of the flow-through design is more appropriate. In the flow-through experiments, a fixed volume (3.251 ml) cylindrical titanium reactor was placed into a gravity-convection Lindberg/Blue oven with temperatures uniformity of 4 ^{o}C at 200 ^{o}C. Aqueous solutions were delivered by a high precision dual-cylinder and gas-tight titanium pump (Quizix SP5000) that provides continuous and pulse-free fluid flow at a constant flow rate. The residence time of the reactant fluids in the cell was controlled by adjusting the flow rate of fluid delivery, which was maintained under constant pressure conditions by an inline backpressure regulator (Coretest DBPR-5). A similar design was adopted by Foustoukos et al. (2007) to evaluate the distribution of trace elements within the two phase region of the NaCl-H_2O system at elevated temperatures and pressures.

In all experiments, dissolved $O_{2(aq)}$ was produced by complete thermal decomposition of dilute $H_2O_{2(aq)}$ aqueous solutions (Sigma-Aldrich), with known starting composition (Table 3, 4). Dissolved H_2 was introduced either by direct injection into the flexible Au/Ti cell, or by purging the reactant solution with H_2 gas at atmospheric pressures prior to delivery by the gas-tight Quizix 5000 pump. Dissolved volatile concentrations were adjusted to reflect the compositional variability expected at near-vent mixing hydrothermal environments. Furthermore, to estimate final mixing ratios needed

143 to properly evaluate the chemical composition of the solution mixture in the batch
144 reactor, the $H_{2(aq)}$-bearing fluids were spiked with 176 ppm of Cl, which served as a
145 conservative chemical tracer. Fluid samples were collected in gas-tight Hamilton locking
146 syringes and then analyzed for dissolved $H_{2(aq)}$, $O_{2(aq)}$ and $N_{2(aq)}$ by a SRI 8610C gas
147 chromatograph equipped with TCD detector and a Carboxen-1010 Plot/Silica-Gel
148 column. Analytical errors are within 5% (2σ) and reflect the larger values of errors
149 between instrument calibration and duplicate analysis of individual samples. Nitrogen
150 concentrations were monitored to account for the atmospheric O_2 contributions
151 introduced during sampling and to adjust accordingly the measured $O_{2(aq)}$ concentrations.
152 Data collected are indicative of minimal air contamination corresponding to very low N_2
153 concentrations (0.2 – 2.7 %). Dissolved chloride concentrations were measured by ion
154 chromatography with estimated uncertainties (2σ) of less than 2%. Fluid pH was
155 measured with a glass combination Thermo-Orion Micro-pH electrode coupled with an
156 Orion Benchtop 250 A pH/mV meter.
157
158 **2.2 Analytical methodology for $H_2O_{2(aq)}$**
159 Dissolved $H_2O_{2(aq)}$ concentrations were retrieved by a Labsystem Multiskan
160 MCC/340 MKII spectrophotometer, following the fluorometric Amplex Red
161 methodology (A-22188 Molecular Probes) with detection limits as low as 50 nmol/kg
162 (ZHOU et al., 1997). This technique involves reaction of H_2O_2 with the Amplex Red
163 reagent (1:1 stoichiometry) and formation of highly fluorescent resorufin under the
164 presence of horseradish peroxidase. The main advantage of the Amplex Red is the low
165 background fluorescence and the enhanced stability of produced resorufin (GOMES et al.,

166 2005, and references therein). A number of studies have shown that Amplex Red is a
167 sensitive and specific probe for the detection of H_2O_2 (COHN et al., 2008;
168 GYULKHANDANYAN and PENNEFATHER, 2004; SEAVER and IMLAY, 2001; SEAVER and
169 IMLAY, 2004).

170 To further establish the accuracy of analytical techniques for hydrogen peroxide
171 detection, a series of flow-through experiments was performed to investigate the kinetics
172 of $H_2O_{2(aq)}$ decomposition in the homogeneous H_2O-$H_2O_{2(aq)}$ system, at temperatures and
173 pressures typical of seafloor mixing hydrothermal environments (60 - 200 ^{o}C, 242 bar)
174 (Table 2). In general, the complete decomposition of $H_2O_{2(aq)}$ is assumed to follow first-
175 order reaction kinetics in keeping with previous studies (CROISET et al., 1997; HIROKI et
176 al., 2002; LIN et al., 1991) and described as:

177 $$H_2O_{2(aq)} \rightarrow H_2O + ½\ O_{2(aq)} \quad (1)$$

178 $$-\frac{d[H_2O_2]}{dt} = k_{H_2O_2}[H_2O_2] \quad (2)$$

179 where k_{H2O2} is the observed decomposition rate coefficient in s^{-1} and t is time in seconds.
180 Results confirm a first-order reaction rate, exhibiting a strong linear correlation between
181 the natural logarithm of $H_2O_{2(aq)}$ concentrations and reaction time giving a slope that
182 defines the k_{H2O2} at each temperature (Fig. 1a). The temperature-dependent decay rate can
183 then be expressed by the Arrhenius equation:

184 $$\ln(k_{H_2O_2}) = \ln(A) - \frac{E_a}{RT} \quad (3)$$

185 where E_a is the activation energy, A is the pre-exponential (or frequency) factor, R is the
186 gas constant (8.314 J mol^{-1} K^{-1}) and T is temperature in Kelvin. The linear temperature
187 dependence of observed k_{H2O2} is in good agreement with previously published data (Fig.

188 1b) (CROISET et al., 1997; LIN et al., 1991), supporting the applicability of experimental
189 and analytical protocols used in this study. The estimated activation energy of 45.1
190 kJ/mole and the pre-exponential factor of 728 s^{-1}, strictly apply to the titanium-bearing
191 flow-through system utilized, but these values are in good agreement with similar data
192 from other studies in which inconel 625 reactors were utilized. In general, reactor surface
193 effects are linked to the oxidation potential of the material and the catalytically enhanced
194 stability of intermediate OH and HO_2 radicals in the H_2O_2 decomposition scheme (HART
195 et al., 1963; HOARE et al., 1967; LIN et al., 1991; TAKAGI and ISHIGURE, 1985). These
196 short-lived radicals would remain absorbed on the metallic surface and likely affect their
197 reactivity potential towards $H_2O_{2(aq)}$ decomposition (LIN et al., 1991). Overall, our results
198 indicate a decrease of the half-life (0.693/ k_{H2O2}) of $H_2O_{2(aq)}$ from 200 min at 60 ^oC to 2
199 min at 200 ^oC, revealing a clear inverse effect of temperature on H_2O_2 stability.
200
201 **3. Results**
202 A total of 6 hydrothermal experiments were performed to assess temperature
203 effects on the rate of the $H_{2(aq)}$-$O_{2(aq)}$ equilibrium at pressures applicable to near-seafloor
204 hydrothermal systems (242-497 bar) (Table 3,4). This redox equilibrium can be
205 expressed by the so-called Knallgas reaction:

206 $$H_{2(aq)} + ½\ O_{2(aq)} \rightarrow H_2O \quad (4)$$

207 It is expected that reaction (4) obeys first-order reaction kinetics with respect to $H_{2(aq)}$
208 abundances, as follows:

209 $$-\frac{d[H_2]}{dt} = k_{H_2}[H_2] \quad (5)$$

where k_{H2} is the decomposition rate coefficient in s^{-1} and t is time in seconds. Data obtained exhibit a strong linear correlation (r^2 = 0.89-0.99) between reaction time and the natural logarithm of the $H_{2(aq)}$ concentrations measured in solution, indicative of a first-order reaction mechanism (Table 3, 4).

In general, results from the flow-through experiments indicate a nearly 39% decrease of dissolved $H_{2(aq)}$ concentrations at 250 ^{o}C within the first 5 minutes of the reaction, consistent with rapid $H_{2(aq)}$-$O_{2(aq)}$ equilibration. Estimated kinetic rate constants at 200 ^{o}C and 250 ^{o}C are 4.11 x 10^{-4} to 5.35 x 10^{-4} s^{-1}, respectively (Table 3, Fig. 2a), and only an order of magnitude slower than the rates of hydrogen peroxide decomposition (Fig. 1b). Thus, at these elevated temperature conditions, trace amounts of $H_2O_{2(aq)}$ may have persisted during the very early stages of reaction with minimal effect on the overall H_2 oxidation process..

Rate constants of the H_2-O_2 equilibrium decreased with decreasing temperatures, ranging from 1.89 x 10^{-4} to 2.69 x 10^{-5} s^{-1} at 125 ^{o}C and 55 ^{o}C respectively, consistent with the abundance of dissolved $H_{2(aq)}$ concentrations, even after several hours of reaction (Table 4). In effect, the first order temperature-dependent rate of $H_{2(aq)}$ oxidation can be described with an activation energy (E_a) of 24 ± 3.4 kJ/mole, and an pre-exponential factor (A) of 6.7 ± 6.7 s^{-1}. Reaction half-life ranges from 22 minutes to 430 minutes at 250 ^{o}C and 55 ^{o}C respectively (Fig. 2).

The relatively high $H_{2(aq)}$ concentrations in these experiments are accompanied by formation of metastable hydrogen peroxide. In fact, dissolved $H_2O_{2(aq)}$ concentrations reached values (0.002 – 0.156 mmol/kg), and persisted in solution for significantly longer reaction times that those predicted from H_2O_2 decomposition rates for the pure H_2O_2-H_2O

system (Fig. 1b). These observations appear to indicate involvement of both $H_{2(aq)}$ and $O_{2(aq)}$ in solution on rate relations (Table 4). Elevated $H_{2(aq)}/O_{2(aq)}$ molar ratios and high $H_{2(aq)}$, concentrations enhance the stability of $H_2O_{2(aq)}$ even at temperatures as high as 125^{o}C. These results are in agreement with previous studies, where comparable amounts of $H_2O_{2(aq)}$ were produced at 100 ^{o}C - 500 bars, under similar compositional constraints (e.g. species concentrations, H_2/O_2 molar ratios) (Table 1) (HOUGHTON, 2003). The fact that hydrothermal formation of hydrogen peroxide is viable at these temperatures and pressures suggests that this species needs to be considered at deep-sea vents. In effect, such enrichments of strong oxidants might inhibit the growth of microbial communities, while the relative distribution of dissolved $H_{2(aq)}$ and $O_{2(aq)}$ could affect the extent of aerobic and anaerobic microbial habitats by defining redox gradients in the near-seafloor hydrothermal vents (EDWARDS et al., 2005; REYSENBACH and SHOCK, 2002).

4. Discussion

4.1 The role of H_2-O_2-H_2O redox equilibria on habitability

The H_2-O_2-H_2O disequilibria observed in this study adds to the distribution of reductants/oxidants in seafloor hydrothermal systems (e.g. $H_{2(aq)}/O_{2(aq)}$, $H_2S_{(aq)}/SO_4^{--}$, Fe^{++}/Fe^{+++}), as well as the overall energy available to microorganisms (MCCOLLOM and SHOCK, 1997). Early models assumed instantaneous equilibration between $H_{2(aq)}$ and $O_{2(aq)}$ and predict an abrupt transition between oxic and anoxic conditions, corresponding to the distribution of redox species in the vent fluid/seawater mixture and the Gibbs (ΔG_r) energy for each redox reaction. Later models recognized the importance of the dependence of the oxic/anoxic interface on the relative abundance of $H_{2(aq)}$ and $O_{2(aq)}$ in

evolved mixture solutions (SHOCK and HOLLAND, 2004). Thus, experimental data demonstrating inhibition of the Knallgas reaction at low temperatures (<150 ^{o}C) will greatly affect the spatial extent of both aerobic and anaerobic bacterial populations in near-seafloor habitats. In fact, the existence of both (hyper)thermophilic and mesophilic hydrogen-oxidizing bacteria utilizing O_2, NO_3^-, and/or S^0 as electron acceptors has been observed in chimney structures and near-vent diffuse flow sites (CAMPBELL et al., 2006; NAKAGAWA and TAKAI, 2008; REYSENBACH and SHOCK, 2002).

Aerobic and anaerobic chemolithoautotrophic microorganisms that thrive in the mixing zone between reducing hydrothermal fluid and oxygenated seawater are highly abundant in a variety of mid-ocean ridge hydrothermal systems. In particular bacteria belonging to the *Epsilonproteobacteria* and *Aquificales* play an important role as primary producers at deep-sea hydrothermal vents (CAMPBELL et al., 2006; NAKAGAWA and TAKAI, 2008; REYSENBACH and SHOCK, 2002). Both groups exhibit similar metabolisms – i.e. the oxidation of reduced sulfur compounds and hydrogen with both oxygen and nitrate or the oxidation of hydrogen with elemental sulfur coupled to the fixation of inorganic carbon – and thus occupy a similar ecological niche. However, they seem to be partitioned by their temperature preference, with *Epsilonproteobacteria* dominating the microbial communities at temperatures from 20 °C to 60 °C, whereas *Aquificae* seem to be the predominant autotrophs at temperatures higher than 60 °C (CAMPBELL et al., 2006; NAKAGAWA and TAKAI, 2008). Different groups of *Epsilonproteobacteria* might also occupy different niches. Members of the *Nautilia*/*Caminibacter* group grow at temperatures between 40 °C and 70 °C, and they rely on hydrogen oxidation coupled to S^0- or nitrate reduction (to NH_4^+) as their energy source. In contrast, members of the

279 *Sulfurimonas* group or the *Sulfurovum* group grow at lower temperatures between 10 °C
280 and 40 °C, and use reduced sulfur compounds and/or molecular hydrogen as electron
281 donors and oxygen or nitrate (to N_2) as electron acceptors (CAMPBELL et al., 2006).
282 Compared to other epsilonproteobacterial isolates, members of these groups can tolerate
283 relatively high amounts of oxygen (NAKAGAWA and TAKAI, 2008); metabolic features
284 that might be beneficial in ecosystems where intensive mixing of hydrothermal fluids and
285 seawater takes place.

286 To better understand the spatial extent of the H_2-O_2 gradient in near-seafloor
287 hydrothermal mixing zones, thermodynamic calculations in the homogeneous H_2-O_2-H_2O
288 system were performed utilizing the experimentally derived kinetic rate law constants (*A*,
289 E_a), while assuming first-order reaction kinetics for the H_2-O_2 redox equilibrium. The
290 reaction path calculations were modeled with Geochemist's Workbench (BETHKE, 1996;
291 BETHKE, 2002), making use of compositional constraints on both seawater and
292 hydrothermal fluid as described by McCollom and Shock (1997). Concentrations of
293 dissolved H_2 for the hydrothermal fluid are lower (1.3 mmol/kg) than in the previous
294 models (1.7 mmol/kgl), accounting for the lack of other competitive oxidation reaction
295 involving Fe^{+2}, $H_2S_{(aq)}$, S^o or Mn^{+2}. Results suggest the presence of a sharp redox gradient
296 at 38 ^oC once conditions reach equilibria (Fig. 3). However, short-term mixing processes
297 allow fluids to achieve simultaneous enrichment in both $H_{2(aq)}$ and $O_{2(aq)}$. For example,
298 even after 10 hours of homogeneous mixing at temperatures as low as 20 ^oC, diffuse flow
299 fluids retain micromolar concentrations of H_2, while shorter reaction times permit more
300 reducing conditions and possibly the establishment of anaerobic zones. Similarly,
301 persistence of dissolved $O_{2(aq)}$ at temperatures higher than 38 ^oC (Fig. 3) could promote

302 growth of microaerophilic chemolithoautotrophs, such as *Aquificaceae and*
303 *Hydrogenothermaceae (e.g. Aquificales)* which grow between 60 °C and 90 °C
304 (NAKAGAWA and TAKAI, 2008).
305
306 *4.1.1 An example: H_2-O_2-H_2O disequilibria and the metabolic pathways of the anaerobic*
307 *nitrate reducers*
308 Biological reduction of dissolved NO_3^- is well known to proceed either through
309 denitrification (i.e. formation of N_2) or ammonification (i.e formation of NH_4^+). In near-
310 seafloor hydrothermal environments, mixing between deep water and high-temperature
311 hydrothermal fluid results in diffuse flow fluids being enriched in NO_3^- (20 - 40 μM in
312 seawater SCHLITZER, 2000) while maintaining moderately high $H_{2(aq)}$ concentrations in
313 accordance with the sluggish kinetics of H_2-O_2 redox equilibrium (Fig. 2). For example,
314 both processes have been suggested to occur at Axial Volcano, Juan de Fuca Ridge,
315 where dissolved NO_3^- concentrations of diffuse flow fluids exhibit depletion from values
316 expected for conservative mixing between seawater and hot hydrothermal fluids, while
317 accompanied by elevated concentrations of ammonia and the presence of nitrous oxide
318 and nitrite (BUTTERFIELD et al., 2004). In line with this observation, a number of
319 mesophilic and thermophilic *Epsilonproteobacteria* and *Aquificales* that perform either
320 denitrification or nitrate ammonification have been isolated from chimney structures and
321 diffuse-flow sites along mid-ocean ridges (ALAIN et al., 2002; GOTZ et al., 2002;
322 MIROSHNICHENKO et al., 2004; NAKAGAWA et al., 2005a; NAKAGAWA et al., 2003;
323 NAKAGAWA et al., 2005b; TAKAI et al., 2004; TAKAI et al., 2006; VETRIANI et al., 2004;
324 VOORDECKERS et al., 2008). Energetically both pathways exhibit similar potential to

support chemolithoautotrophic metabolism (STROHM et al., 2007). Denitrification, however, has been shown to proceed under microaerobic conditions despite the potentially inhibiting role of $O_{2(aq)}$ on anaerobic denitrifying activity (DAVIES et al., 1989; HERNANDEZ and ROWE, 1987; MCKENNEY et al., 2001).

Overall, the range of $O_{2(aq)}$ concentrations that anaerobic NO_3^- reducers can tolerate spans between 2 and 54 μM (GOTZ et al., 2002; NAKAGAWA et al., 2003; NAKAGAWA et al., 2005b; TAKAI et al., 2004; TAKAI et al., 2006). These concentrations would reflect important fractions of seawater (100 - 250 μM $O_{2(aq)}$ SCHLITZER, 2000) in the low-temperature diffuse flow fluids and would contribute to strong redox gradients along the mixing interface. Thermodynamic calculations on the energetic contributions of the excess dissolved $O_{2(aq)}$ to the Knallgas reaction performed at 70 ^oC - 250 bars suggest that it is the strongly out-of equilibrium $O_{2(aq)}$ concentrations that would account for most of the bioavailable energy and not the concentration of dissolved $H_{2(aq)}$, even when the latter ranges from 100 μM to 10 mM (Fig. 4). Thus, the tendency of denitrifiers to switch between aerobic and anaerobic metabolism and to carry out nitrate reduction in the presence of $O_{2(aq)}$ likely imposes an important constraint on microbial diversity at near-seafloor hydrothermal sites as they can out compete organisms executing ammonification under these conditions. On the other hand, under low nitrate concentrations, such as expected at higher temperatures (i.e. elevated contribution of hydrothermal fluid in diffuse flow), nitrate ammonification has been found to allow a higher growth yield than denitrification (STROHM et al., 2007). Consequently, one could expect that organisms carrying out ammonification have a competitive advantage under these conditions. Currently, no conclusive data on the relative abundance of denitrifiers and ammonifiers at

348 different temperatures exist, but existing data on cultures are generally supportive of this
349 trend (CAMPBELL et al., 2006).
350
351 **4.2 Formation of metastable $H_2O_{2(aq)}$**
352 A number of studies have focused on the formation of hydrogen peroxide in
353 aqueous solutions through different reaction mechanisms. For example in Borda et al.
354 (2003), addition of pyrite grains to O_2-free water appeared to enhance adsorption of H_2O
355 and ferric Fe at sulfur-deficient lattice sites resulting in the possible formation of
356 metastable hydroxyl radicals and $H_2O_{2(aq)}$. Similarly, by applying mechanical or electric
357 charge stresses in silicate minerals, O_2-defect lattice sites bearing O^- species might be
358 formed, leading to oxidation of H_2O to H_2O_2 through formation of O radicals (BALK et
359 al., 2009; HUROWITZ et al., 2007). In addition, direct formation of $H_2O_{2(aq)}$ through $H_{2(aq)}$
360 oxidation by dissolved O_2 is promoted in the presence of Pd or Au-Pd supported catalyst
361 ($T < 25\ ^oC$) (CHINTA and LUNSFORD, 2004; DISSANAYAKE and LUNSFORD, 2002;
362 DISSANAYAKE and LUNSFORD, 2003; EDWARDS et al., 2009; LANDON et al., 2003;
363 LUNSFORD, 2003; POSPELOVA et al., 1961). Reaction pathways that lead to direct $H_2O_{2(aq)}$
364 formation involve the hydrogenation of oxygen and H_2 activation to form an HO_2 surface
365 intermediate, with H_2O_2 decomposition to H_2O being inhibited, especially when
366 dissolved halides are in solution (Cl^-, Br^-, F^-, I^-) (EDWARDS et al., 2008; LUNSFORD, 2003;
367 POSPELOVA and KOBOZEV, 1961). Dissolved halides minimize the rate of H_2O_2
368 decomposition by changing the electronic properties of the catalyst and by eliminating
369 active lattice sites (CHOUDHARY and SAMANTA, 2006; CHOUDHARY et al., 2007). Thus, in
370 the homogeneous H_2-O_2-H_2O system of our study, the trace amounts of dissolved Cl^-

371 used as chemical tracer likely had little effect on the yield of hydrogen peroxide
372 synthesis. In deep sea hydrothermal environments, however, circulation of evolved
373 seawater might play a role in enhancing the stability of hydrogen peroxide possibly
374 formed in near-seafloor mixing zones. Likewise the surface of the Au/Ti reaction cell did
375 not affect reactions, as native Au has been shown to be chemically inert (HAN et al.,
376 2007), with TiO_2 exhibiting minimal effects on $H_2O_{2(aq)}$ decomposition (HIROKI et al.,
377 2002; LIN et al., 1991).

378 In our study, synthesis of metastable $H_2O_{2(aq)}$ occurred at low temperature
379 hydrothermal conditions ($T < 150\ ^oC$) and in the absence of mineral or metal catalytic
380 surfaces. The stability of H_2O_2 appears to be associated with the availability of both $H_{2(aq)}$
381 and $O_{2(aq)}$ in solution, further supporting the role of H_2-O_2 redox disequilibrium in
382 promoting synthesis of metastable oxidants. In effect, concentrations of H_2O_2 attained
383 were significantly higher than those expected based on the kinetic rate of direct H_2O_2
384 decomposition and maintained constant along extensive reaction times (~ hrs) (Fig. 5)
385 (Table 4). Elevated $H_{2(aq)}/O_{2(aq)}$ molar ratios and high $H_{2(aq)}$ concentrations enhance
386 $H_2O_{2(aq)}$ formation, even at temperatures as high as 130^oC (Fig. 5), suggesting that
387 conditions of elevated reduction potential might be required to facilitate synthesis of
388 strong oxidants. This is consistent with previous studies proposing that $H_{2(aq)}/O_{2(aq)}$ molar
389 ratios might play a role in controlling the relative rates of the two competing reaction
390 pathways of interest: H_2 oxidation to H_2O and/or H_2O_2 (CHINTA and LUNSFORD, 2004).
391 In this reaction scheme, hydrogen peroxide is considered an intermediate/metastable
392 phase towards water formation, and thus, it requires presence of both $H_{2(aq)}$ and $O_{2(aq)}$. In
393 effect, synthesis of $H_2O_{2(aq)}$ has been described as a hydrogenation reaction of O_2 to

394 account for the stability of the O-O relative to the weak H-H bonds (EDWARDS et al.,
395 2008).

396 Evidence for the catalytic effects of the elevated $H_{2(aq)}/O_{2(aq)}$ ratios provides an
397 explanation of the existence of dissolved H_2O_2 in the 95 ^{o}C experiment. For example,
398 $H_{2(aq)}$ injection after nearly 24 hrs of reaction resulted in a significant increase of $H_2O_{2(aq)}$,
399 the concentration of which eventually decreased following the gradual removal of $O_{2(aq)}$
400 through $H_{2(aq)}$ oxidation (Fig. 6). Accordingly H_2O_2 decomposition through
401 hydrogenation to H_2O ($H_{2(aq)} + H_2O_{2(aq)} \rightarrow H_2O$) is kinetically favored over direct
402 decomposition to H_2O and to trace amounts of $O_{2(aq)}$, when compared to conditions prior
403 to $O_{2(aq)}$ elimination. This is in agreement with previous observations (CHINTA and
404 LUNSFORD, 2004; LANDON et al., 2003; POSPELOVA et al., 1961). Here, H_2O radiolysis
405 has been proposed to support communities of thermophilic H_2-utilizing and sulfate
406 reducing bacteria, without any apparent mechanism to allow removal of the oxidant
407 radiolysis byproducts (e.g. H_2O_2) (LIN et al., 2005; LIN et al., 2006). The strong effect of
408 $H_{2(aq)}$ in enhancing H_2O_2 decomposition under anaerobic conditions, as observed in our
409 experiments, could potentially serve this role and in this way reduce oxidative stress for
410 organisms living in such deep crustal fractures, in line with genomic data indicating a
411 limited machinery to cope with oxidative stress (CHIVIAN et al., 2008).

412 The counteracting oxidative effects of hydrogen peroxide occurrence under
413 reducing conditions is completely unknown and might alter the extent of the oxic-anoxic
414 zones developed during mixing of high-temperature anoxic hydrothermal fluid and cold
415 oxygenated seawater at near-seafloor environments. Experimental data showing
416 hydrothermal formation of $H_2O_{2(aq)}$ at temperatures and pressures typical of seafloor vent

environments could support the presence of dissolved $H_2O_{2(aq)}$ in low-temperature diffuse fluids. In light of these results, we note that a number of hydrothermal vent bacteria, encompassing obligate anaerobes, potentially living in this mixing zone have been shown to have mechanisms to cope with oxidative stress, including the scavenging of endogenous H_2O_2 (CAMPBELL et al., 2009; MARKERT et al., 2007; NAKAGAWA et al., 2007; VETRIANI et al., 2004; VOORDECKERS et al., 2008).

The possibility of $H_2O_{2(aq)}$ coexisting with Fe-oxides or dissolved Fe^{+2} at seafloor hydrothermal vents, could also provide a suitable catalytic substrate to promote formation of hydroxyl radicals (•OH). Possible reactions that facilitate radical formation in place of a non-radical $H_2O_{2(aq)}$ decomposition to $O_{2(aq)}$ and H_2O (Eq. 1), are closely related to the general scheme of Fenton-type chemistry (KWAN and VOELKER, 2003):

$$Fe^{+2} + H_2O_{2(aq)} \rightarrow Fe^{+3} + OH^- + \bullet OH \qquad (6)$$

This is a well-known reaction used extensively in environmental engineering for wastewater remediation, where formation of •OH enables the chemical oxidation of organic contaminants. While the reaction commonly involves Fe^{+2} dissolved in solution, magnetite has been shown to be the most catalytically effective Fe-oxide reactant, mainly due to coexistence of Fe^{+2} and Fe^{+3} on the octahedral sites of the mineral lattice (COSTA et al., 2006; MOURA et al., 2006). A recent experimental study has indeed demonstrated the role of magnetite-catalyzed Fenton reaction in promoting $H_2O_{2(aq)}$ decomposition and hydroxyl radical formation under low temperature hydrothermal conditions (80-150 ^oC; 172-241 bar) (FOUSTOUKOS AND STERN, 2010). Undoubtedly, the likelihood of dissolved hydroxyl radicals being stable in diffuse flow fluids, when coexisting with Fe-oxides, has important implications for a number of geochemical and biochemical processes occurring

in near-seafloor hydrothermal sites. Fluxes of such strong oxidants (e.g. H_2O_2, •OH) will impose significant constraints on redox conditions in seawater/hydrothermal fluid mixtures, affecting not only the kinetic rates of homogeneous $H_{2(aq)}$ oxidation, but also the distribution of dissolved alkanes and carboxylic acids in diffuse flow hydrothermal vent fluids. This process may be important in decreasing the flux of dissolved organic carbon (DOC) in low-temperature vent fluids, and thus, serve as a plausible mechanism to explain the DOC-depleted diffuse fluids sampled at Bay Bare Seamount and ODP Hole 1026B; off-axis sites near Juan de Fuca Ridge (LANG et al., 2006).

5. Conclusions

We conducted a series of open and closed system experiments utilizing flow-though and flexible Au/Ti reaction cells to examine the effect of temperature on $H_{2(aq)}$-$O_{2(aq)}$ equilibria. These experiments involved mixing of $H_{2(aq)}$- and $O_{2(aq)}$-bearing aqueous solutions at temperature and pressure conditions reflecting near-seafloor hydrothermal environments (55-250 ^{o}C and 242-497 bar). This fundamental redox equilibria expressed through the Knallgas reaction has been shown to proceed instantaneously to thermodynamic equilibrium at elevated temperatures and pressures (SEEWALD, 1994). Results in our experiments, however, revealed that $H_{2(aq)}$ oxidation is inhibited as temperature decreases, allowing for development of excess $H_{2(aq)}$ in solution and, most importantly, promoting the stability of hydrogen peroxide as a metastable intermediate phase evolving along the reaction pathway for water formation.

The slow reaction rate of $H_{2(aq)}$-$O_{2(aq)}$ redox equilibrium and the synthesis of hydrogen peroxide at low temperatures may influence the oxidation of dissolved organic

463 species in an unpredictable way. For example, the relatively sluggish rate of oxidation of
464 short-chain alkanes predicted for low temperature chemical alteration can be overturned
465 by the oxidation effects of such a strong oxidant. Thus, formation of hydrogen peroxide
466 during H_2-O_2-H_2O disequilibria at temperatures lower than 130^{o}C suggests that the
467 oxidation of alkanes could occur under hydrothermal conditions, providing a possible
468 mechanism to produce molecules that have relevance for prebiotic chemistry, such as
469 methanol and formaldehyde that serve as intermediates during methane oxidation to CO_2
470 and CO. Formation of these metastable phases at low temperatures will provide new
471 insights on the availability of complex organic compounds in hydrothermal environments
472 and impose important constraints on the habitability of other planetary bodies containing
473 liquid water.
474
475 *Acknowledgements:* This research was conducted with partial support from the NSF
476 OCE-0752221 and the Geophysical Laboratory Postdoctoral Fellowship. We would also
477 like to acknowledge contributions by the W.M. Keck Foundation and Shell towards
478 supporting the hydrothermal lab at the Geophysical Lab. SMS acknowledges support
479 from NSF OCE-0452333 and the Alfried-Krupp Wissenschaftskolleg Greifswald
480 (Germany), while WES acknowledges support from NSF grants OCE-0549457 and OCE-
481 0813861. Finally, we would like to thank the contributions and comments from the
482 Associate Editor, Dr. J. Alt and three anonymous reviewers.

Table 1. Distribution of dissolved H_2 and $O_{2(aq)}$ in fluid samples retrieved from hydrothermal experiments at 100 ^{o}C and 500 bar (Houghton, 2003).

Reaction time (hrs)	$H_{2aq)}$ (mmol/kg)	$O_{2aq)}$ (mmol/kg)	Rate constant (k_{H2}) (s^{-1})
0	2.012	1.104	$5.45 \times 10^{-5} \pm 1.7 \times 10^{-6}$
0.5	1.443	0.809	$r^2 = 0.84$
2	0.976	0.023	
4	0.865	n.d.	

Table 2. Results of flow-through experiments on $H_2O_{2(aq)}$ decomposition at 60-200 °C and 242 bar.

	Fluid flow rate (ml/min)	Reaction time (sec)	$H_2O_{2(aq)}$ (mmol/kg)	2σ [a] (mmol/kg)	Rate constant (k) (s^{-1})
T = 60 °C					$5.77 \times 10^{-5} \pm 2.310^{-5}$
	start		1.995	0.02	$r^2 = 0.47$
	0.66	310	1.752	0.02	
	0.66	310	1.845	0.02	
	0.33	621	1.686	0.02	
	0.33	621	1.845	0.02	
	0.22	931	1.799	0.02	
	0.22	931	1.750	0.02	
	0.11	1862	1.656	0.02	
	0.11	1862	1.732	0.02	
T = 90 °C					$2.48 \times 10^{-4} \pm 6.9 \times 10^{-5}$
	start		1.092	0.012	$r^2 = 0.72$
	0.685	299	1.010	0.016	
	0.685	299	1.032	0.012	
	0.228	898	0.666	0.012	
	0.228	898	0.860	0.012	
	0.114	1796	0.733	0.012	
	0.114	1796	0.673	0.012	
T = 120 °C					$1.43 \times 10^{-3} \pm 5.8 \times 10^{-5}$
	start		1.995	0.02	$r^2 = 0.99$
	0.66	310	1.255	0.02	
	0.66	310	1.415	0.061	
	0.33	621	1.108	0.015	
	0.33	621	1.065	0.063	
	0.22	931	0.545	0.02	
	0.22	931	0.677	0.02	
	0.11	1862	0.159	0.02	
T = 150 °C					$2.11 \times 10^{-3} \pm 2.3 \times 10^{-4}$
	start		1.092	0.012	$r^2 = 0.95$
	1.37	149	0.853	0.012	
	0.685	299	0.583	0.012	
	0.685	299	0.591	0.012	
	0.342	599	0.363	0.04	
	0.342	599	0.290	0.04	
T = 180 °C					$4.29 \times 10^{-5} \pm 3.3 \times 10^{-4}$
	start		1.995	0.02	$r^2 = 0.98$
	1.32	155	0.951	0.02	
	1.32	155	0.913	0.02	
	0.66	310	0.545	0.02	
	0.66	310	0.479	0.02	

T = 200 ^{o}C					$5.51 \times 10^{-3} \pm 3.1 \times 10^{-4}$
	start		1.092	0.012	$r^2 = 0.99$
	1.32	155	0.951	0.02	
	1.32	155	0.913	0.02	
	0.66	310	0.545	0.02	
	0.66	310	0.479	0.02	

[a] Analytical errors reported are the larger values of errors associated with instrument calibration and duplicate analysis of individual samples.

The volume of the titanium reactor, including tubing situated within the high temperature zone, is 3.413 ml.

483

Table 3. Concentrations of dissolved $H_{2(aq)}$ and $H_2O_{2(aq)}$ measured in samples collected during flow-through experiments on H_2 oxidation at 200-250 °C and 242 bar.

	Fluid flow rate (ml/min)	Reaction time (sec)	$H_{2aq)}$ (mmol/kg)	$H_2O_{2(aq)}$ (mmol/kg)	2σ [a] (mmol/kg)	pH (25 °C)	Rate constant (k_{H2}) (s^{-1})
T = 200 °C							$4.11 \times 10^{-4} \pm 4.0 \times 10^{-5}$
start (25 °C)	2	102	0.638	2.249	0.009	5.9	$r^2 = 0.93$
start (25 °C)	2	102	0.646	2.341	0.009	6.0	
	2	102	0.596	1.136	0.012	6.0	$k_{H2O2} = 1.63 \times 10^{-2} \pm 8.5 \times 10^{-3}$
	0.678	300	0.515	0.079	0.007	6.6	$r^2 = 0.55$
	0.678	300	0.549	0.061	0.001	6.1	
	0.678	300	0.542	0.021	0.007	6.5	
	0.226	900	0.435	*b.d.*		6.4	
	0.226	900	0.456	*b.d.*		5.8	
	0.226	900	0.426	*b.d.*		6.2	
	0.226	900	0.455	*b.d.*		6.2	
T = 250 °C							$5.35 \times 10^{-4} \pm 3.2 \times 10^{-5}$
start (25 °C)	2	102	0.638	2.410	0.033	6.0	$r^2 = 0.98$
start (25 °C)	2	102	0.627	2.495	0.035	6.2	
	2	102	0.602	0.205	0.014	6.3	$k_{H2O2} = 1.71 \times 10^{-2} \pm 4.3 \times 10^{-3}$
	2	102	0.605	0.212	0.024	6.2	$r^2 = 0.76$
	0.685	297	0.514	*n.a.*		6.5	
	0.685	297	0.499	0.019	0.029	6.5	
	0.685	297	0.541	0.005	0.008	6.3	
	0.228	892	0.380	*b.d.*		6.6	
	0.228	892	0.398	*b.d.*		6.7	
	0.228	892	0.391	*b.d.*		6.4	

[a] Analytical errors reported are the larger values of errors associated with instrument calibration and duplicate analysis of individual samples.

Errors for dissolved $H_{2(aq)}$ analysis are ± 5%. The volume of the titanium reactor, including tubing situated within the high temperature zone, is 3.390 ml.

b.d.: below detection limit

n.a.: not analyzed

Table 4. Concentrations of dissolved aqueous species during H_2 oxidation in closed system hydrothermal experiments at 55-130 °C and 297-497 bar.

	P (bar)	Reaction time (min)	$H_{2aq)}$ (mmol/kg)	$O_{2aq)}$ (mmol/kg)	$H_2O_{2(aq)}$ (mmol/kg)	2σ [a] (mmol/kg)	pH (25 °C)	Cl [c] (ppm)	Rate constant (k_{H2}) (s^{-1})
T = 55 °C									$2.69 \times 10^{-5} \pm 3.2 \times 10^{-6}$
start					8.00	0.04	5.8	15	$r^2 = 0.94$
	234	874		4.00[b]	*b.d.*		6.1		
	299	895		4.00[b]	*b.d.*		5.8		
Injection of aqueous solution containing 32 mmol/kg $H_{2(aq)}$ – Final concentration of 4.45 mmol/kg									
	326	92	3.99	3.44[b]	*b.d.*		6.7		
	299	135	3.84	*n.a*	*b.d.*		6.8	42	
	276	185	3.01	*n.a*	*b.d.*		6.6		
	315	241	2.89	*n.a*	*b.d.*		6.3		
	308	347	2.43	*n.a*	*b.d.*		6.2	37	
	276	427	2.40	*n.a*	*b.d.*		6.3		
T = 130 °C									$7.63 \times 10^{-5} \pm 1.1 \times 10^{-5}$
start					7.92	0.04	5.0	16	$r^2 = 0.89$
	411	110		3.96[b]	*b.d.*				
Injection of aqueous solution containing 32 mmol/kg $H_{2(aq)}$ – Final concentration of 4.51 mmol/kg									
	307	47	3.15	3.40[b]	0.008	0.0002	5.6	28	
	355	62	2.86	*n.a*	0.012	0.0003	5.6		
	335	92	2.62	*n.a*	0.008	0.0002	5.7		
	328	107	2.17	*n.a*	0.018	0.0003	5.4		
	320	122	2.77	*n.a*	0.015	0.0002	5.5	27	
	302	152	2.11	*n.a*	0.010	0.0002	5.6	32	
	329	182	1.77	*n.a*	0.009	0.0002	5.4		
T = 125 °C									$1.89 \times 10^{-4} \pm 4.3 \times 10^{-6}$
start					12.39	0.12	4.5		$r^2 = 0.99$
	397	133		5.86	*b.d.*		6.0	13	
	383	139		5.94	*b.d.*				
Injection of aqueous solution containing 40 mmol/kg $H_{2(aq)}$ – Final concentration of 5.9 mmol/kg									
	424	42	4.61	4.23	0.113	0.0004	5.9		
	435	57	2.54	2.92	0.110	0.0003	6.0		
	401	68	2.76	3.32	0.124	0.0009	6.1		
	393	87	2.04	2.80	0.077	0.0003	*n.a*	34	
	343	129	1.31	2.41	0.051	0.0007	6.0		
	450	157	0.965	2.04	0.038	0.0003	*n.a*		
	364	184	0.677	2.32	0.025	0.0002	5.9		
	395	213	0.480	2.13	0.029	0.0002	6.0		
	402	242	0.337	1.84	0.006	0.0002	6.0		
	391	291	0.245	1.71	0.008	0.0002	5.7	28	
	397	335	0.129	2.21	0.005	0.0002	5.9		
	355	391	0.060	1.66	*b.d.*		*n.a*		
	329	421	0.058	2.14	*b.d.*		*n.a*		

T = 95 °C								$4.37 \times 10^{-5} \pm 3.7 \times 1\ 0^{-6}$
start				11.81	0.12	4.7		$r^2 = 0.94$
	499	171	4.85	*b.d.*		5.6	11	
	468	184	4.82	*b.d.*				
Injection of aqueous solution containing 53 mmol/kg $H_{2(aq)}$ – Final concentration of 8.0 mmol/kg								
	497	50	7.46	4.48	0.064	0.0008	6.0	
	450	79	6.43	3.86	0.123	0.0002	6.0	
	456	105	5.19	3.28	0.154	0.0011	5.9	36
	439	134			0.149	0.0004	*n.a*	
	458	149	5.42	3.36	0.154	0.0010	5.9	
	457	182	5.06	3.24	0.172	0.0010	5.8	
	409	211	4.22	2.85	0.148	0.0002	*n.a*	
	412	240	4.55	3.09	0.145	0.0002	5.9	28
	428	252	4.05	2.65	0.147	0.0004	*n.a*	33
	403	289	3.47	2.48	0.156	0.0002	6.0	
	419	322	3.57	2.71	0.118	0.0002	5.9	
	440	360	2.27	1.88	0.100	0.0008	5.9	
	411	1426	0.388	1.33	0.013	0.0003	*n.a*	
	389	1451	0.365	1.22	0.011	0.0002	6.7	35
Injection of aqueous solution containing 45 mmol/kg $H_{2(aq)}$ – Final concentration of 8.16 mmol/kg								
	471	29	8.73	0.44	0.047	0.0004	6.8	
	435	110	3.68	0.42	0.048	0.0002	*n.a*	
	411	123	4.46	0.10	0.036	0.0002	6.9	67
	428	154	6.46		0.003	0.0001	6.7	64
	447	163	5.40		*b.d.*		*n.a*	

[a] Analytical errors reported are the larger values of errors associated with instrument calibration and duplicate analysis of individual samples. Errors for dissolved $H_{2(aq)}$ and $O_{2(aq)}$ analysis are ± 5%. Oxygen compositions have been adjusted to account for contributions from atmospheric O_2.

[b] Dissolved O_2 concentrations estimated assuming complete decomposition of $H_2O_{2(aq)}$

[c] Dissolved chloride concentration in the injected aqueous solution is 176 ppm. Fluids were spiked with chloride to better constrain final mixing ratios in the batch reactor, and estimate the dissolved H_2 concentrations attained immediately after injection of the H_2-bearing aqueous solutions.

b.d.: below detection limit

n.a.: not analyzed

484
485
486

487

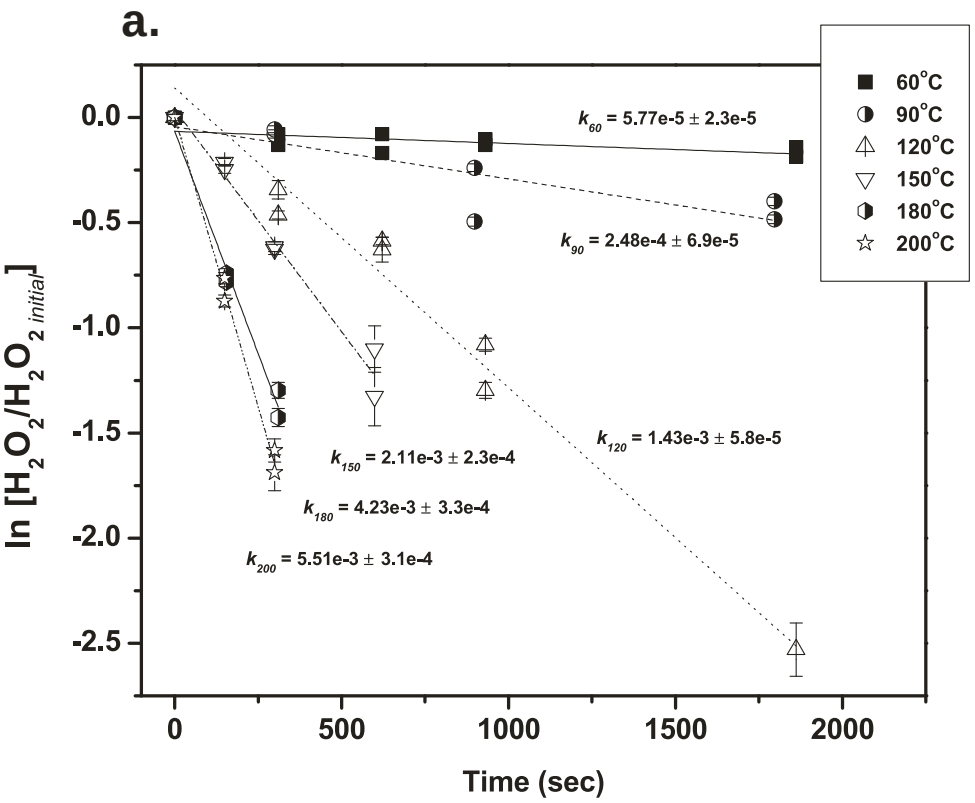
a.
60°C
90°C
120°C
150°C
180°C
200°C
k_{60} = 5.77e-5 ± 2.3e-5
k_{90} = 2.48e-4 ± 6.9e-5
k_{120} = 1.43e-3 ± 5.8e-5
k_{150} = 2.11e-3 ± 2.3e-4
k_{180} = 4.23e-3 ± 3.3e-4
k_{200} = 5.51e-3 ± 3.1e-4
ln [$H_2O_2/H_2O_{2\ initial}$]
Time (sec)

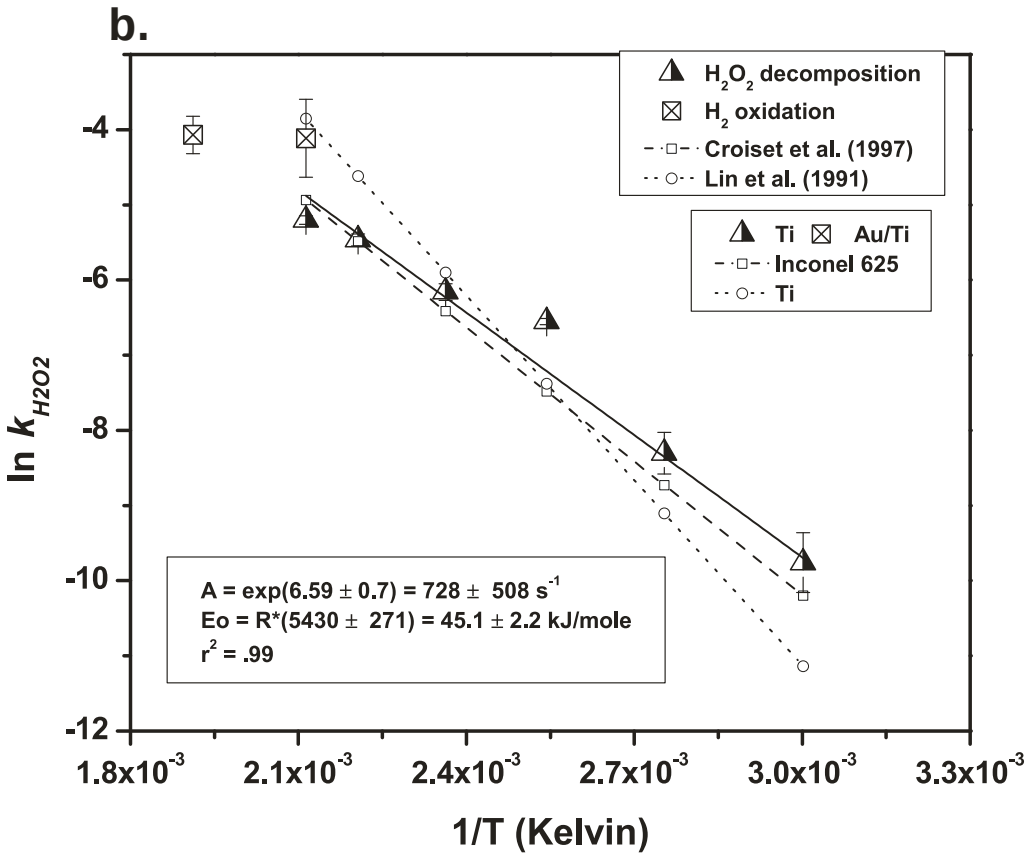
b.
H_2O_2 decomposition
H_2 oxidation
Croiset et al. (1997)
Lin et al. (1991)
Ti
Au/Ti
Inconel 625
Ti
A = exp(6.59 ± 0.7) = 728 ± 508 s^{-1}
Eo = R*(5430 ± 271) = 45.1 ± 2.2 kJ/mole
r^2 = .99
ln k_{H2O2}
1/T (Kelvin)

488

Figure 1. Decomposition of $H_2O_{2(aq)}$ in the homogeneous H_2O_2-H_2O system at 60-200 ^oC and 242 bar. (a) Experimental data indicate first-order reaction rate supported by the linear correlation between the natural logarithm values of $H_2O_{2(aq)}$ concentrations and reaction time. The slope of the line defines the kinetic rate constant (k_{H2O2}) at a range of temperatures, and allows temperature-dependent decay rates to be described in an Arrhenius plot (b). Results are in good agreement with previous studies of H_2O_2 decomposition that involved titanium and Inconel 625 reactors. Furthermore, rates of H_2O_2 decay in the H_2-enriched experiments conducted by utilizing a flexible Au/Ti reaction cell at temperatures of 200-250 ^oC (Table 3), are consistent with the kinetic rate law constants (A, E_a) determined from the lower temperature experimental data.

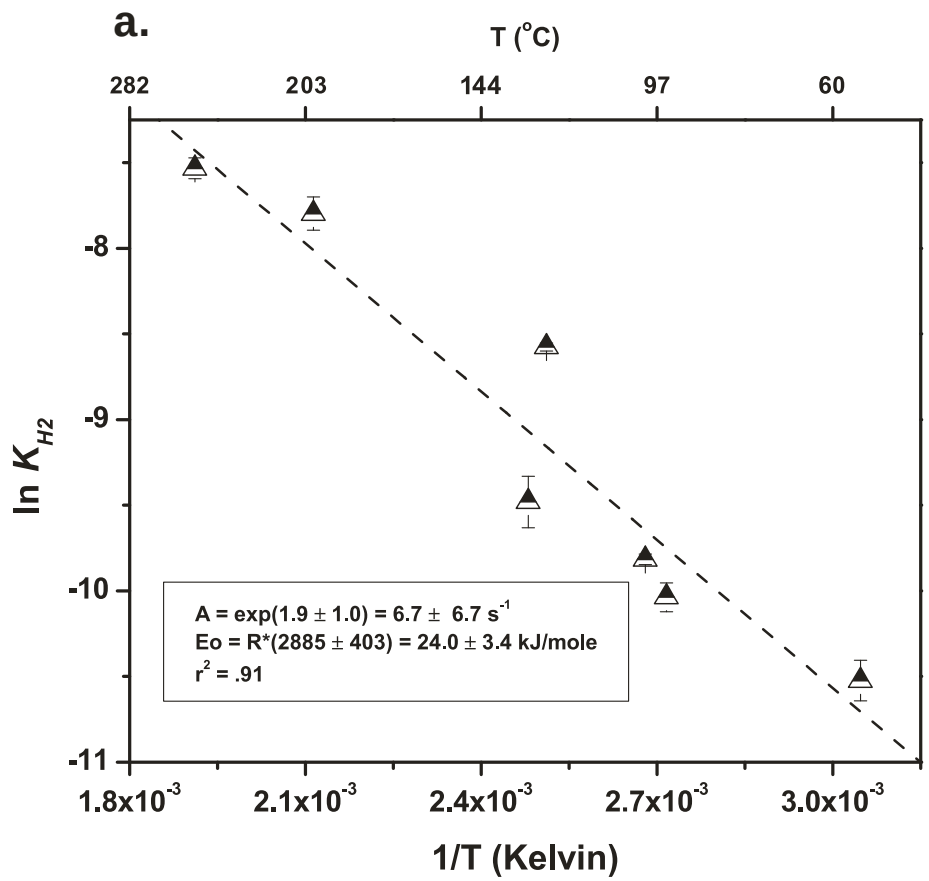
a.
T (°C)
282
203
144
97
60
-8
-9
-10
-11
ln K_{H2}
A = exp(1.9 ± 1.0) = 6.7 ± 6.7 s^{-1}
Eo = R*(2885 ± 403) = 24.0 ± 3.4 kJ/mole
r^2 = .91
1.8x10^{-3}
2.1x10^{-3}
2.4x10^{-3}
2.7x10^{-3}
3.0x10^{-3}
1/T (Kelvin)

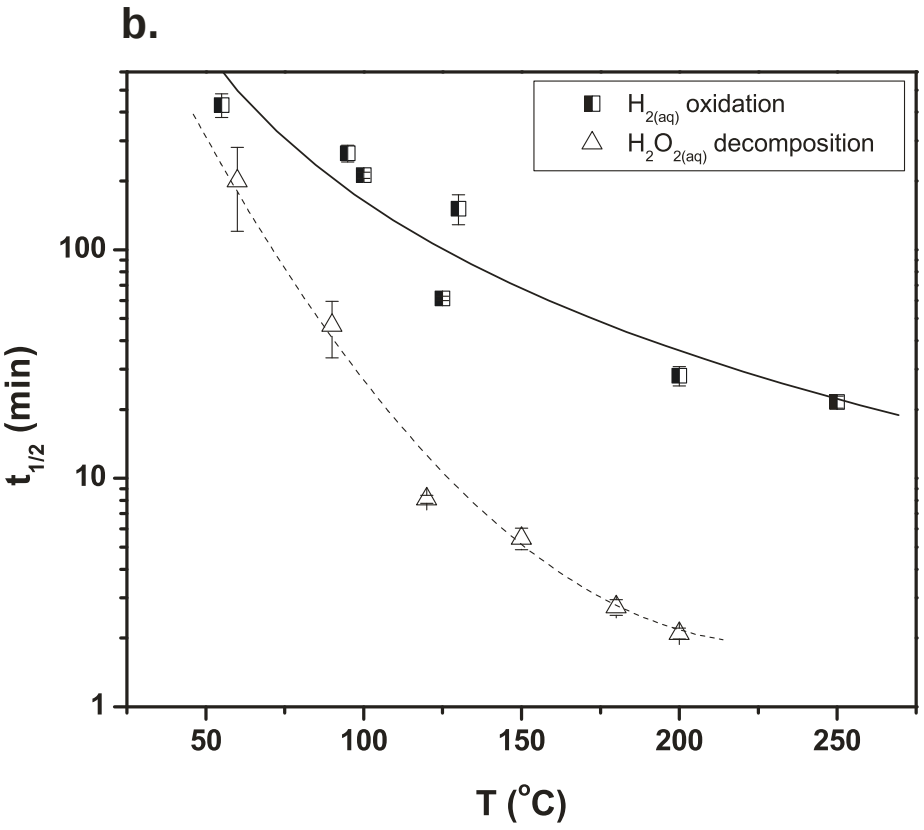
b.
$H_{2(aq)}$ oxidation
$H_2O_{2(aq)}$ decomposition
100
10
1
$t_{1/2}$ (min)
50
100
150
200
250
T (°C)

501

Figure 2. Arrhenius plot and rate constants of H_2 oxidation in presence of dissolved $O_{2(aq)}$ at temperatures ranging from 55°C to 250°C and pressures of 242 - 497 bar. (a). The first order temperature-dependent oxidation rate of $H_{2(aq)}$ is described with an activation energy (E_a) of 24 ± 3.4 kJ/mole and an pre-exponential factor (A) of 6.7 ± 6.7 s^{-1}, resulting in reaction half-times that range from 22 minutes to 430 minutes at 250°C and 55°C respectively. Arrhenius parameters also include the kinetic rate constant measured at 100°C – 500 bar by Houghton (2003) (Table 1). (b). Experimental observations and model results provide evidence of strong H_2-O_2 disequilibrium at low temperatures that allows excess $H_{2(aq)}$ and establishment of highly reducing conditions. Estimated half-life of $H_2O_{2(aq)}$ decay is nearly an order of magnitude lower than that of $H_{2(aq)}$ oxidation and is approximately 200 and 2 min at 60°C and 200°C, respectively.

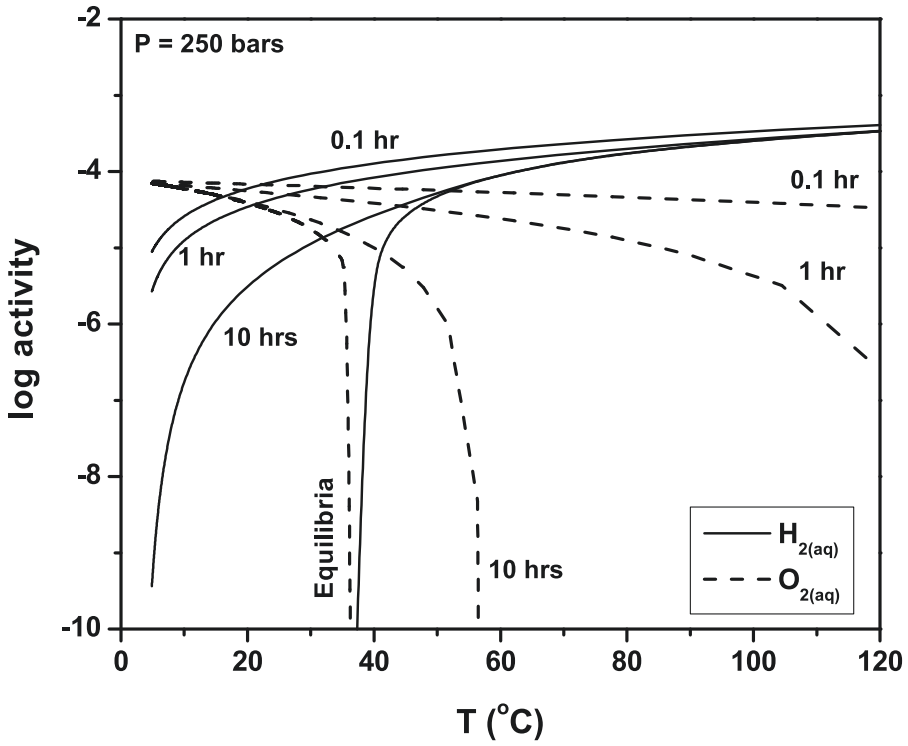

Figure 3. Theoretical modeling of the distribution of $H_{2(aq)}$ and $O_{2(aq)}$ during mixing between high-temperature $H_{2(aq)}$-enriched hydrothermal fluid and oxygenated seawater, performed with compositional constraints described by McCollom and Shock (1997), while utilizing the experimentally derived kinetic rate of H_2 oxidation from the present study. Equilibrium conditions develop a sharp redox gradient at 38°C, in agreement with previous studies (McCollom and Shock, 1997). Mixing processes occurring at different residence times (0.1-10 hrs), however, reveal formation of fluids highly enriched in both $H_{2(aq)}$ and $O_{2(aq)}$ at a range of temperatures, weakening the presence of a sharp oxic/anoxic interface. This, in turn, might have important implications for the distribution of anaerobic, microaerophilic and aerobic chemolithoautotrophs at diffuse flow vent sites and within near-vent subsurface environments by allowing for enhanced microbial diversity at a wide range of temperature and redox conditions.

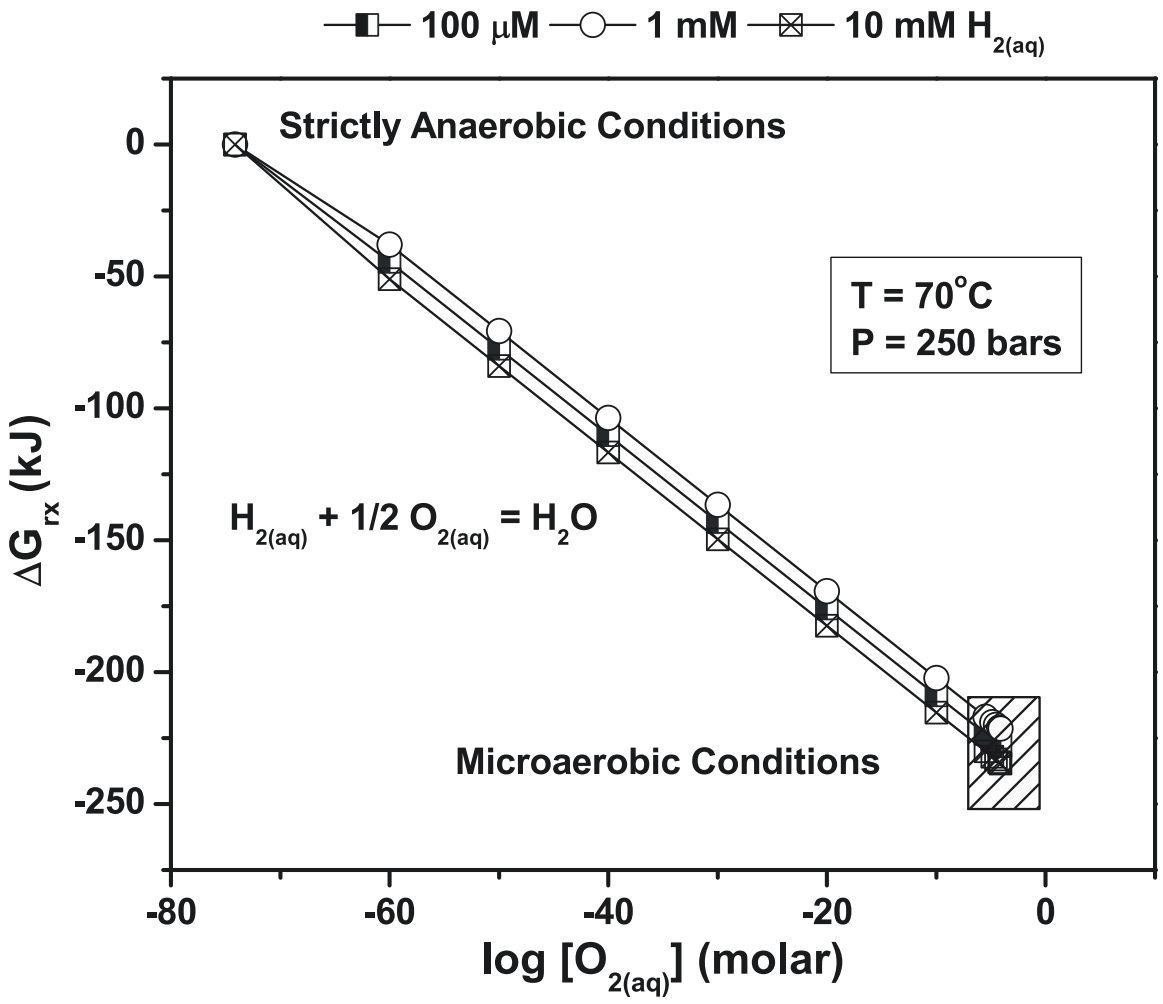

Figure 4. Energetics of the Knallgas reaction as function of available $O_{2(aq)}$ in solution. Under equilibrium conditions, abundant presence of $H_{2(aq)}$ at concentrations ranging from 100 μM to 100 mM results in strictly anaerobic conditions. The presence of microaerobic $O_{2(aq)}$ concentrations reflecting the tolerance limits of NO_3-reducers (2 - 54 μM) (shaded box), however, has a great affinity to provide bioavailable energy at levels that permit respiratory denitrification to be more favorable over ammonification. Thus, the adaptability of anaerobic microorganisms to utilize trace amounts of $O_{2(aq)}$ might greatly affect microbial diversity at subsurface habitats as it can control metabolic pathways (e.g. denitrification vs ammonification) developed along complex and dynamic redox gradients. Gibbs energy calculations for the Knallgas reaction were performed following

methodologies discussed in other theoretical studies (MCCOLLOM and SHOCK, 1997; SHOCK and HOLLAND, 2004).

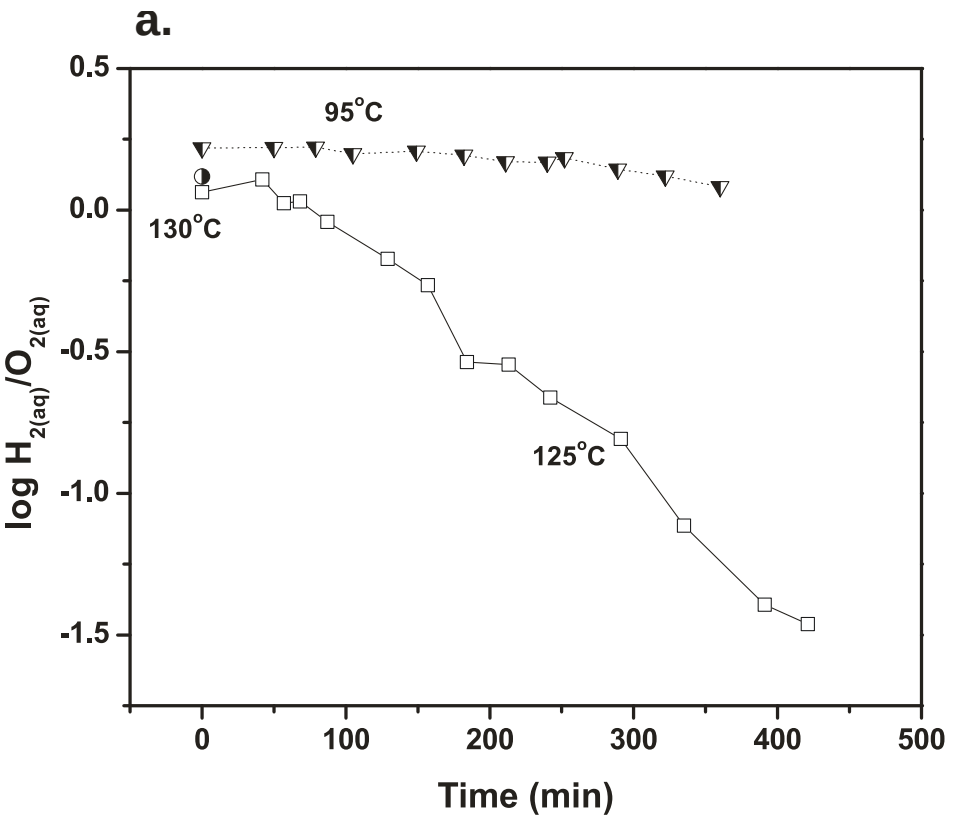
a.
95°C
130°C
125°C
log H2(aq)/O2(aq)
Time (min)
0.5
0.0
-0.5
-1.0
-1.5
0
100
200
300
400
500

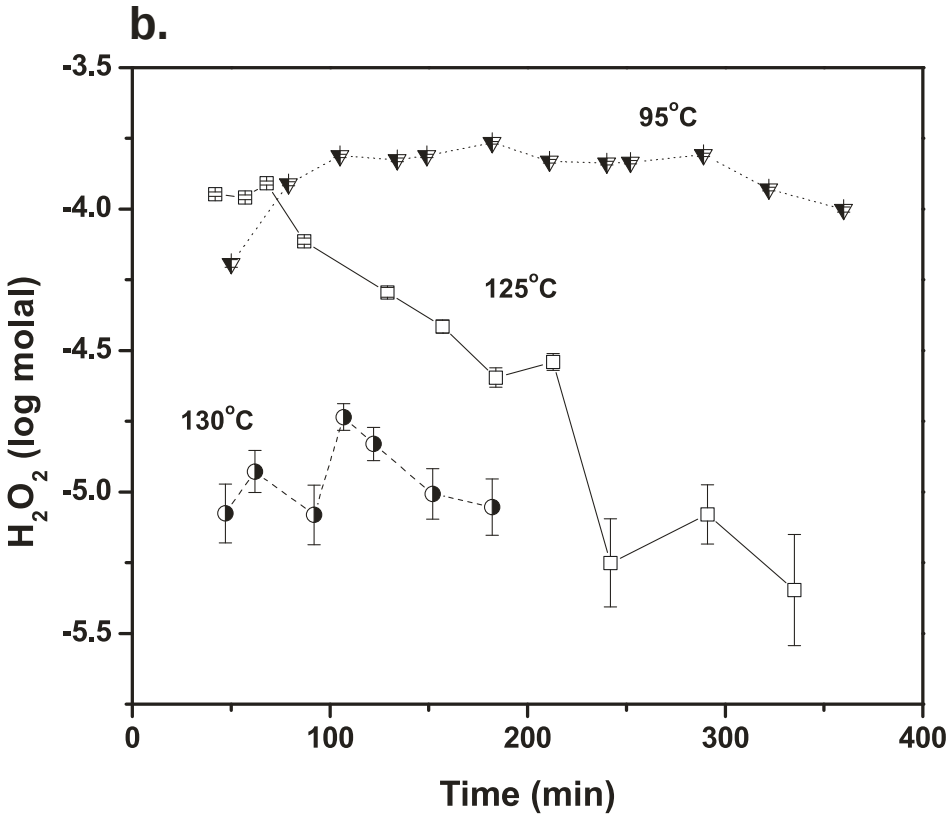
b.
95°C
125°C
130°C
H2O2 (log molal)
Time (min)
-3.5
-4.0
-4.5
-5.0
-5.5
0
100
200
300
400

539
540

Figure 5. Experimental results of metastable $H_2O_{2(aq)}$ formation under elevated H_2/O_2 molar ratios and temperatures between 95 ^oC and 130 ^oC (242-497 bar). Dissolved $H_2O_{2(aq)}$ concentrations attained values (0.002 – 0.156 mmol/kg) significantly higher than those predicted based on rates of direct H_2O_2 decomposition to H_2O and $O_{2(aq)}$. The yield of $H_2O_{2(aq)}$ is dependent on both $H_{2(aq)}$ and $O_{2(aq)}$ concentrations. However, highly reducing conditions appear to increase the extent of metastable equilibria between H_2, O_2 and H_2O_2. Under these conditions, direct decomposition of hydrogen peroxide is suppressed and the $H_2O_{2(aq)}$ hydrogenation to H_2O might have reached a steady-state condition likely due to the presence of highly enriched $H_{2(aq)}$ solutions. This is clearly demonstrated at 95 ^oC, where elevated H_2/O_2 molar ratios were sustained for reaction times of nearly 24 hrs.

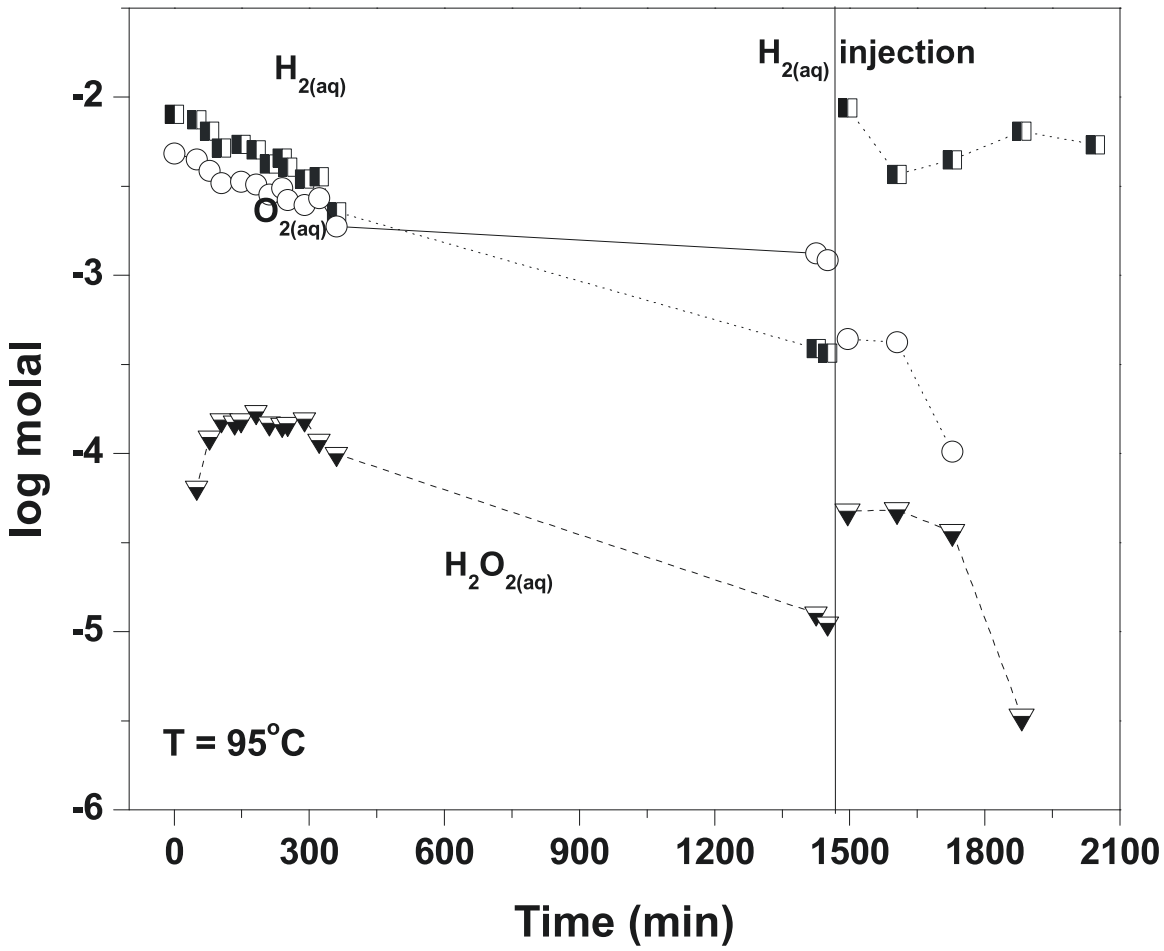

Figure 6. The catalytic effect of elevated $H_{2(aq)}/O_{2(aq)}$ ratios on enhancing synthesis of H_2O_2 at low temperature hydrothermal conditions. Injection of $H_{2(aq)}$ in the Au/Ti reaction cell after nearly 24 hrs of H_2 oxidation at 95 ^{o}C resulted in a significant increase in dissolved $H_2O_{2(aq)}$ concentrations, supporting the effect of elevated $H_{2(aq)}/O_{2(aq)}$ on the yield of dissolved oxidants. Furthermore, results are indicative of kinetically favored H_2O_2 decomposition through the reaction pathway involving hydrogenation to H_2O based on the elimination of $H_2O_{2(aq)}$ observed after $O_{2(aq)}$ removal from solution. In effect, this might have implications for the habitability of deep crustal environments controlled by the distribution of H_2O radiolysis products (e.g. H_2, H_2O_2, OH radicals) and the availability of electron donors for anaerobic metabolism (e.g. H_2), such as the volcanic units in the Witwatersrand Basin, South Africa.

564
565 **REFERENCES**
566

567 Alain, K., Querellou, J., Lesongeur, F., Pignet, P., Crassous, P., Raguenes, G., Cueff, V.,
568 and Cambon-Bonavita, M. A., 2002. *Caminibacter hydrogeniphilus* gen. nov., sp
569 nov., a novel thermophilic, hydrogen-oxidizing bacterium isolated from an East
570 Pacific Rise hydrothermal vent. *Int. J. Syst. Evol. Microbiol.* **52**, 1317-1323.
571 Balk, M., Bose, M., Ertem, G., Rogoff, D. A., Rothschild, L. J., and Freund, F. T., 2009.
572 Oxidation of water to hydrogen peroxide at the rock-water interface due to stress-
573 activated electric currents in rocks. *Earth Planet. Sci. Lett.* **283**, 87-92.
574 Bethke, C. M., 1996. *Geochemical reaction modeling: Concepts and applications*.
575 Oxford University Press, New York, 397 pp..
576 Bethke, C. M., 2002. *The Geochemist's WorkbenchTM, version 4.0, A User's Guide to*
577 *Rxn, Act2, React, and Gtplot*, University of Illinois, Urbana, IL.
578 Borda, M. J., Elsetinow, A. R., Strongin, D. R., and Schoonen, M. A., 2003. A
579 mechanism for the production of hydroxyl radical at surface defect sites on pyrite.
580 *Geochim. Cosmochim. Acta* **67**, 935-939.
581 Butterfield, D. A., Lilley, M. D., Huber, J., Roe, K. K., Embley, R. W., and Massoth, G.
582 J., 2004. Mixing, reaction and microbial activity in the sub-seafloor revealed by
583 temporal and spatial variation in diffuse flow vents at axial volcano. In: Wilcock,
584 W. S. D., DeLong, E. F., Kelley, D. S., Baross, J. A., and Cary, S. C. Eds.), *The*
585 *Subsurface Biosphere at Mid-Ocean Ridges, AGU Monograph 144, pp. 269-289.*
586 Campbell, B. J., Engel, A. S., Porter, M. L., and Takai, K., 2006. The versatile epsilon-
587 proteobacteria: key players in sulphidic habitats. *Nat. Rev. Microbiol.* **4**, 458-468.
588 Campbell, B. J., Smith, J. L., Hanson, T. E., Klotz, M. G., Stein, L. Y., Lee, C. K., Wu,
589 D. Y., Robinson, J. M., Khouri, H. M., Eisen, J. A., and Cary, S. C., 2009.
590 Adaptations to submarine hydrothermal environments exemplified by the genome
591 of Nautilia profundicola. *Plos Genetics* **5**, e1000362,
592 doi:10.1371/journal.pgen.1000362.
593 Chinta, S. and Lunsford, J., 2004. A mechanistic study of H_2O_2 and H_2O formation from
594 H_2 and O_2 catalyzed by palladium in an aqueous medium. *J. Catal.* **225**, 249-255.
595 Chivian, D., Brodie, E.L., Alm, E.J., Culley, D.E., Dehal, P.S., DeSantis, t.Z., Gihring,
596 T.M., Lapidus, A., Lin, L., and et al. 2008, Environmental genomics reveals a
597 single-species ecosystem deep within Earth. *Science*, **322**, 275-278.
598 Choudhary, V. R. and Samanta, C., 2006. Role of chloride or bromide anions and protons
599 for promoting the selective oxidation of H_2 by O_2 to H_2O_2 over supported Pd
600 catalysts in an aqueous medium. *J. Catal.* **238**, 28-38.
601 Choudhary, V. R., Samanta, C., and Jana, P., 2007. Formation from direct oxidation of
602 H-2 and destruction by decomposition/hydrogenation of $_{H2O2}$ over Pd/C catalyst in
603 aqueous medium containing different acids and halide anions. *Appl. Catal., A*
604 **317**, 234-243.
605 Cohn, C. A., Simon, S. R., and Schoonen, M. A. A., 2008. Comparison of fluorescence-
606 based techniques for the quantification of particle-induced hydroxyl radicals.
607 *Part. Fibre Toxicol.* **5**, doi:10.1186/1743-8977-5-2.

608 Corliss, J. B., Dymond, J., Gordon, L. I., Edmond, J. M., Von Herzen, R. P., Ballard, R.
609 D., Green, K., Williams, D., Bainbridge, A., and et al., 1979. Submarine thermal
610 springs on the Galapagos Rift. *Science* **203**, 1073-83.
611 Costa, R. C. C., Lelis, M. F. F., Oliveira, L. C. A., Fabris, J. D., Ardisson, J. D., Rios, R.
612 R. V. A., Silva, C. N., and Lago, R. M., 2006. Novel active heterogeneous Fenton
613 system based on $Fe_{3-x}M_xO_4$ (Fe, Co, Mn, Ni): The role of M^{2+} species on the
614 reactivity towards H_2O_2 reactions. *J. Hazard. Mater.* **129**, 171-178.
615 Croiset, E., Rice, S. F., and Hanush, R., 1997. Hydrogen peroxide decomposition in
616 supercritical water. *AIChe* **43**, 2343-2352.
617 Davies, K. J. P., Lloyd, D., and Boddy, L., 1989. The effect of oxygen on denitrification
618 in Paracoccus-Denitrificans and Pseudomonas-Aeruginosa. *J. Gen. Microbiol.*
619 **135**, 2445-2451.
620 Ding, K., Seyfried, W. E., Jr., Tivey, M. K., and Bradley, A. M., 2001. In-situ
621 measurement of dissolved H_2 and H_2S in high-temperature hydrothermal vent
622 fluids at the main Endeavour Field, Juan de Fuca Ridge. *Earth Planet. Sci. Lett.*
623 **186**, 417-425.
624 Ding, K., Seyfried, W. E. J., Zhang, Z., Tivey, M. K., Von Damm, K. L., and Bradley, A.
625 M., 2005. The in-situ pH of hydrothermal fluids at mid-ocean ridges. *Earth*
626 *Planet. Sci. Lett.* **237**, 167-174.
627 Dissanayake, D. P. and Lunsford, J. H., 2002. Evidence for the role of colloidal
628 palladium in the catalytic formation of H_2O_2 from H_2 and O_2. *J. Catal.* **206**, 173-
629 176.
630 Dissanayake, D. P. and Lunsford, J. H., 2003. The direct formation of H_2O_2 from H_2 and
631 O_2 over colloidal palladium. *J. Catal.* **214**, 113-120.
632 Edmond, J. M., Measures, C., Mangum, B., Grant, B., Sclater, F. R., Collier, R., Hudson,
633 A., Gordon, L. I., and Corliss, J. B., 1979. On the formation of metal-rich deposits
634 at ridge crests. *Earth Planet. Sci. Lett.* **46**, 19-30.
635 Edwards, J. K., Carley, A. F., Herzing, A. A., Kiely, C. J., and Hutchings, G. J., 2008.
636 Direct synthesis of hydrogen peroxide from H_2 and O_2 using supported Au-Pd
637 catalysts. *Faraday Discuss.* **138**, 225-239.
638 Edwards, J. K., Solsona, B., N, E. N., Carley, A. F., Herzing, A. A., Kiely, C. J., and
639 Hutchings, G. J., 2009. Switching off hydrogen peroxide hydrogenation in the
640 direct synthesis process. *Science* **323**, 1037-1041.
641 Edwards, K. J., Bach, W., and McCollom, T., 2005. Geomicrobiology in oceanography:
642 microbe-mineral interactions at and below the seafloor. *Trends Microbiol.* **13**,
643 doi:10.1016/J.tim.2005.07.005.
644 Foustoukos, D. I. and Seyfried, W. E., 2007. Trace element partitioning between vapor,
645 brine and halite under extreme phase separation conditions. *Geochim.*
646 *Cosmochim. Acta* **71**, 2056-2071.
647 Foustoukos, D. I. and Stern, J.C. 2010. Oxidation of organics under hydrothermal
648 conditions: Implications for the evolution of methane on Mars, *Twelveth Annual*
649 *V. M. Goldschmidt Conference.* Knoxville, TN, #A302 (abstr.).
650 Foustoukos, D. I., Seyfried, W. E., Jr., Ding, K., and Pester, N. J., 2009. Dissolved
651 carbon species in associated diffuse and focused flow hydrothermal vents at the
652 Main Endeavour Field, northern Juan de Fuca ridge. *Geochem. Geophys. Geosyst.*
653 **10**, Q10003, doi:10.1029/2009GC002472.

Gomes, A., Fernandes, E., and Lima, J. L. F. C., 2005. Fluorescence probes used for detection of reactive oxygen species. *J. Biochem. Bioph. Methods* **65**, 45-80.

Gotz, D., Banta, A., Beveridge, T. J., Rushdi, A. I., Simoneit, B. R. T., and Reysenbach, A., 2002. *Persephonella marina* gen. nov., sp nov and *Persephonella guaymasensis* sp nov., two novel, thermophilic, hydrogen-oxidizing microaerophiles from deep-sea hydrothermal vents. *Int. J. Syst. Evol. Microbiol.* **52**, 1349-1359.

Gyulkhandanyan, A. V. and Pennefather, P. S., 2004. Shift in the localization of sites of hydrogen peroxide production in brain mitochondria by mitochondrial stress. *J. Neurochem.* **90**, 405-421.

Han, Y. F., Zhong, Z. Y., Ramesh, K., Chen, F. X., Chen, L. W., White, T., Tay, Q. L., Yaakub, S. N., and Wang, Z., 2007. Au promotional effects on the synthesis of H_2O_2 directly from H_2 and O_2 on supported Pd-Au alloy catalysts. *J. Phys. Chem. C* **111**, 8410-8413.

Hart, A. B., Mcfadyen, J., and Ross, R. A., 1963. Solid-oxide-catalyzed decomposition of hydrogen peroxide vapour. *Trans. Faraday Soc.* **59**, 1458-&.

Hernandez, D. and Rowe, J. J., 1987. Oxygen regulation of nitrate uptake in denitrifying Pseudomonas-Aeruginosa. *Appl. Environ. Microbiol.* **53**, 745-750.

Hiroki, A., Pimblott, S. M., and LaVerne, J. A., 2002. Hydrogen peroxide production in the radiolysis of water with high radical scavenger concentrations. *J. Phys. Chem. A* **106**, 9352-9358.

Hoare, D. E., Peacock, G. B., and Ruxton, G. R. D., 1967. Efficiency of surfaces in destroying hydrogen peroxide and hydroperoxyl radicals. *Tran. Faraday Soc.* **63**, 2498-&.

Houghton, J. L., 2003. Biogeochemistry of seafloor hydrothermal vent systems : an experimental study conducted at in situ conditions, PhD Thesis, University of Minnesota, MN, USA.

Hurowitz, J. A., Tosca, N. J., McLennan, S. M., and Schoonen, M. A. A., 2007. Production of hydrogen peroxide in Martian and lunar soils. *Earth Planet. Sci. Lett.* **255**, 41-52.

Kamei, G. and Ohmoto, H., 2000. The kinetics of reactions between pyrite and O_2-bearing water revealed from in situ monitoring of DO, Eh and pH in a closed system. *Geochim. Cosmochim. Acta* **64**, 2585-2601.

Kelley, D. S., Baross, J. A., and Delaney, J. R., 2002. Volcanoes, fluids, and life at mid-ocean ridge spreading centers. *Annu. Rev. Earth Planet. Sci.* **30**, 385-491.

Kwan, W. P. and Voelker, B. M., 2003. Rates of hydroxyl radical generation and organic compound oxidation in mineral-catalyzed Fenton-like systems. *Environ. Sci. Technol.* **37**, 1150-1158.

Landon, P., Collier, P. J., Carley, A. F., Chadwick, D., Papworth, A. J., Burrows, A., Kiely, C. J., and Hutchings, G. J., 2003. Direct synthesis of hydrogen peroxide from H_2 and O_2 using Pd and Au catalysts. *Phys. Chem. Chem. Phys.* **5**, 1917-1923.

Lang, S. Q., Butterfield, D. A., Lilley, M. D., Johnson, P., and Hedges, J. I., 2006. Dissolved organic carbon in ridge-axis and ridge-flank hydrothermal systems. *Geochim. Cosmochim. Acta* **15**, 3830-3842.

699 Lin, C. C., Smith, F. R., Ichikawa, N., Baba, T., and Itow, M., 1991. Decomposition of
700 hydrogen peroxide in aqueous solutions at elevated temperatures. *Int. J. Chem.*
701 *Kinet.* **23**, 971-987.
702 Lin, L. H., Hall, J., Lippmann-Pipke, J., Ward, J. A., Lollar, B. S., DeFlaun, M., Rothmel,
703 R., Moser, D., Gihring, T. M., Mislowack, B., and Onstott, T. C., 2005. Radiolytic
704 H_2 in continental crust: Nuclear power for deep subsurface microbial
705 communities. *Geochem. Geophys. Geosyst.* **6**, Q07003,
706 doi:10.1029/2004GC000907.
707 Lin, L. H., Wang, P. L., Rumble, D., Lippmann-Pipke, J., Boice, E., Pratt, L. M., Lollar,
708 B. S., Brodie, E. L., Hazen, T. C., Andersen, G. L., DeSantis, T. Z., Moser, D. P.,
709 Kershaw, D., and Onstott, T. C., 2006. Long-term sustainability of a high-energy,
710 low-diversity crustal biome. *Science* **314**, 479-482.
711 Lindberg, R. D. and Runnells, D. D., 1984. Groundwater redox reactions - an analysis of
712 equilibrium state applied to Eh measurements and geochemical modeling. *Science*
713 **225**, 925-927.
714 Lunsford, J. H., 2003. The direct formation of H_2O_2 from H_2 and O_2 over palladium
715 catalysts. *J. Catal.* **216**, 455-460.
716 Luther, G. W., Glazer, B. T., Hohmann, L., Popp, J. I., Taillefert, M., Rozan, T. F.,
717 Brendel, P. J., Theberge, S. M., and Nuzzio, D. B., 2001. Sulfur speciation
718 monitored in situ with solid state gold amalgam voltammetric microelectrodes:
719 polysulfides as a special case in sediments, microbial mats and hydrothermal vent
720 waters. *J. Environ. Monit.* **3**, 61-66.
721 Markert, S., Arndt, C., Felbeck, H., Becher, D., Sievert, S. M., Hugler, M., Albrecht, D.,
722 Robidart, J., Bench, S., Feldman, R. A., Hecker, M., and Schweder, T., 2007.
723 Physiological proteomics of the uncultured endosymbiont of Riftia pachyptila.
724 *Science* **315**, 247-250.
725 McCollom, T. M. and Seewald, J. S., 2006. Carbon isotope composition of organic
726 compounds produced by abiotic synthesis under hydrothermal conditions. *Earth*
727 *Planet. Sci. Lett.* **243**, 74-84.
728 McCollom, T. M. and Shock, E. L., 1997. Geochemical constraints on
729 chemolithoautotrophic metabolism by microorganisms in seafloor hydrothermal
730 systems. *Geochim. Cosmochim. Acta* **61**, 4375-4391.
731 McKenney, D. J., Drury, C. F., and Wang, S. W., 2001. Effects of oxygen on
732 denitrification inhibition, repression, and derepression in soil columns. *Soil Sci.*
733 *Soc. Am. J.* **65**, 126-132.
734 Miroshnichenko, M. L., L'Haridon, S., Schumann, P., Spring, S., Bonch-Osmolovskaya,
735 E. A., Jeanthon, C., and Stackebrandt, E., 2004. Caminibacter profundus sp nov.,
736 a novel thermophile of Nautiliales ord. nov within the class
737 'Epsilonproteobacteria', isolated from a deep-sea hydrothermal vent. *Int. J. Syst.*
738 *Evol. Microbiol.* **54**, 41-45.
739 Moura, F. C. C., Oliveira, G. C., Araujo, M. H., Ardisson, J. D., Macedo, W. A. A., and
740 Lago, R. M., 2006. Highly reactive species formed by interface reaction between
741 Fe-0-iron oxides particles: An efficient electron transfer system for environmental
742 applications. *Appl. Catal. A* **307**, 195-204.
743 Nakagawa, S., Inagaki, F., Takai, K., Horikoshi, K., and Sako, Y., 2005a. Thioreductor
744 micantisoli gen. nov., sp nov., a novel mesophilic, sulfur-reducing

chemolithoautotroph within the epsilon-Proteobacteria isolated from hydrothermal sediments in the Mid-Okinawa Trough. *Int. J. Syst. Evol. Microbiol.* **55**, 599-605.

Nakagawa, S. and Takai, K., 2008. Deep-sea vent chemoautotrophs: diversity, biochemistry and ecological significance. *FEMS Microbiol. Ecol.* **65**, 1-14.

Nakagawa, S., Takai, K., Horikoshi, K., and Sako, Y., 2003. Persephonella hydrogeniphila sp nov., a novel thermophilic, hydrogen-oxidizing bacterium from a deep-sea hydrothermal vent chimney. *Int. J. Syst. Evol. Microbiol.* **53**, 863-869.

Nakagawa, S., Takai, K., Inagaki, F., Horikoshi, K., and Sako, Y., 2005b. Nitratiruptor tergarcus gen. nov., sp nov and Nitratifractor salsuginis gen. nov., sp nov., nitrate-reducing chemolithoautotrophs of the epsilon-Proteobacteria isolated from a deep-sea hydrothermal system in the Mid-Okinawa Trough. *Int. J. Syst. Evol. Microbiol.* **55**, 925-933.

Nakagawa, S., Takaki, Y., Shimamura, S., Reysenbach, A. L., Takai, K., and Horikoshi, K., 2007. Deep-sea vent epsilon-proteobacterial genomes provide insights into emergence of pathogens. *Proc. Natl. Acad. Sci. USA* **104**, 12146-12150.

Pospelova, T. A. and Kobozev, N. I., 1961. Palladium catalyzed synthesis of hydrogen peroxide from the elements 2. The active centers of palladium in the synthesis of H_2O_2. *Zhurnal Fizicheskoi Khimii* **35**, 535-542.

Pospelova, T. A., Kobozev, N. I., and Eremin, E. N., 1961. Palladium catalyzed synthesis of hydrogen peroxide from the elements .1. Conditions for the formation of hydrogen peroxide. *Zhurnal Fizicheskoi Khimii* **35**, 298-305.

Reysenbach, A.-L., Banta, A. B., and Luther, G., 2000. Microbial essentials at vents. *Nature* **404**, 835.

Reysenbach, A.-L. and Shock, E., 2002. Merging genomes with geochemistry in hydrothermal ecosystems. *Science* **296**, 1077.

Schlitzer, R., 2000. Electronic atlas of WOCE hydrographic and tracer data now available. *Eos Trans. AGU* **81**, 45.

Seaver, L. C. and Imlay, J. A., 2001. Hydrogen peroxide fluxes and compartmentalization inside growing Escherichia coli. *J. Bacteriol*. **183**, 7182-7189.

Seaver, L. C. and Imlay, J. A., 2004. Are respiratory enzymes the primary sources of intracellular hydrogen peroxide? *J. Biol. Chem.* **279**, 48742-48750.

Seewald, J., 1994. Evidence for metastable equilibriuum between hydrocarbons under hydrothermal conditions. *Nature* **370**, 285-287.

Seewald, J. S., Zolotov, M. Y., and McCollom, T., 2006. Experimental investigation of single carbon compounds under hydrothermal conditions. *Geochim. Cosmochim. Acta* **70**, 446-460.

Seyfried, W. E. J., Janecky, D. R., and Berndt, M. E., 1987. Rocking autoclaves for hydrothermal experiments: II. The flexible reaction-cell system. In: H. Barnes and Ulmer, G. Eds.), *Hydrothermal Experimental Techniques*. Wiley-Interscience, New York.

Shock, E. L. and Holland, H. D., 2004. Geochemical energy sources that support the subsurface biosphere. In: Wilcock, W. S. D., DeLong, E. F., Kelley, D. S., Baross, J. A., and Cary, S. C. Eds.), *The Subsurface Biosphere at Mid-Ocean Ridges, AGU Monograph 144*, 153-165.

790 Strohm, T. O., Griffin, B., Zumft, W. G., and Schink, B., 2007. Growth yields in bacterial
791 denitrification and nitrate ammonification. *Appl. Environ. Microbiol.* **73**, 1420-
792 1424.
793 Takagi, J. and Ishigure, K., 1985. Thermal-decomposition of hydrogen-peroxide and its
794 effect on reactor water monitoring of boiling water-reactors. *Nuclear Sci. Eng.* **89**,
795 177-186.
796 Takai, K., Nealson, K. H., and Horikoshi, K., 2004. *Hydrogenimonas thermophila* gen.
797 nov., sp nov., a novel thermophilic, hydrogen-oxidizing chemolithoautotroph
798 within the epsilon-Proteobacteria, isolated from a black smoker in a Central
799 Indian Ridge hydrothermal field. *Int. J. Syst. Evol. Microbiol.* **54**, 25-32.
800 Takai, K., Suzuki, M., Nakagawa, S., Miyazaki, M., Suzuki, Y., Inagaki, F., and
801 Horikoshi, K., 2006. *Sulfurimonas paralvinellae* sp nov., a novel mesophilic,
802 hydrogen- and sulfur-oxidizing chemolithoautotroph within the Epsilonproteo-
803 bacteria isolated from a deep-sea hydrothermal vent polychaete nest,
804 reclassification of *Thiomicrospira denitrificans* as *Sulfurimonas denitrificans*
805 comb. nov and emended description of the genus Sulfurimonas. *Int. J. Syst. Evol.*
806 *Microbiol.* **56**, 1725-1733.
807 Tivey, M. K., 1995. The influence of hydrothermal fluid composition and advection rates
808 on black smoker chimney mineralogy: insights from modeling transport and
809 reaction. *Geochim. Cosmochim. Acta* **59**, 1933-49.
810 Vetriani, C., Speck, M. D., Ellor, S. V., Lutz, R. A., and Starovoytov, V., 2004.
811 *Thermovibrio ammonificans* sp nov., a thermophilic, chemolithotrophic, nitrate-
812 ammonifying bacterium from deep-sea hydrothermal vents. *Int. J. Syst. Evol.*
813 *Microbiol.* **54**, 175-181.
814 Voordeckers, J. W., Do, M. H., Hugler, M., Ko, V., Sievert, S. M., and Vetriani, C.,
815 2008. Culture dependent and independent analyses of 16S rRNA and ATP citrate
816 lyase genes: a comparison of microbial communities from different black smoker
817 chimneys on the Mid-Atlantic Ridge. *Extremophiles* **12**, 627-640.
818 Zhou, M., Diwu, Z., Panchuk-Voloshina, N., and Haugland, R., 1997. A stable
819 nonfluorescent derivative of resorufin for the fluorometric determination of trace
820 hydrogen peroxide: Applications in detecting the activity of phagocyte NADPH
821 oxidase and other oxidases. *Anal. Biochem.* **253**, 162-168.
822
823